Two distinct ubiquitin-binding motifs in A20 mediate its anti-inflammatory and cell- protective activities

Arne Martens[1,2], Dario Priem[1,2], Esther Hoste[1,2], Jessica Vetters[1,3], Sofie Rennen[1,3], Leen Catrysse[1,2], Sofie Voet[1,2], Laura Deelen[1,2], Mozes Sze[1,2], Hanna Vikkula[1,2], Karolina Slowicka[1,2], Tino Hochepied[1,2], Kalliopi Iliaki[4], Andy Wullaert[1,2,3], Sophie Janssens[1,3], Mohamed Lamkanfi[1,3,5], Rudi Beyaert[1,2], Marietta Armaka[4], Mathieu JM Bertrand[1,2] and Geert van Loo[1,2]

[1] *VIB Center for Inflammation Research, B-9052 Ghent, Belgium.*

[2] *Department of Biomedical Molecular Biology, Ghent University, B-9052 Ghent, Belgium.*

[3] *Department of Internal Medicine and Pediatrics, Ghent University, Ghent, Belgium.*

[4] *Biomedical Sciences Research Center 'Alexander Fleming', G-16672 Vari, Greece*

[5] *Janssen Immunosciences, World without Disease Accelerator, Pharmaceutical Companies of Johnson & Johnson, B-2340 Beerse, Belgium*

Correspondence: Geert van Loo (geert.vanloo@irc.vib-ugent.be), Center for Inflammation Research, VIB and Ghent University, Technologiepark 71, B-9052 Ghent, Belgium. Fax: 003292217673; Tel: 0032-93313761.

Abstract

Protein ubiquitination regulates protein stability and modulates the composition of signaling complexes. A20 is a negative regulator of inflammatory signaling, but the molecular mechanisms involved are ill-understood. Here, we generated *Tnfaip3* gene-targeted A20 mutant mice bearing inactivating mutations in the zinc finger 7 (ZnF7) and ZnF4 ubiquitin-binding domains, revealing that binding to polyubiquitin is essential for A20 to suppress inflammatory disease. We demonstrate that a functional ZnF7 domain was required for recruiting A20 to the tumor necrosis factor receptor 1 (TNFR1) signaling complex and to suppress inflammatory signaling and cell death. The combined inactivation of ZnF4 and ZnF7 phenocopied the postnatal lethality and severe multi-organ inflammation of A20-deficient mice. Conditional tissue-specific expression of mutant A20 further revealed the key role of ubiquitin-binding in myeloid and intestinal epithelial cells. Collectively, these results demonstrate that the anti-inflammatory and cytoprotective functions of A20 are largely dependent on its ubiquitin-binding properties.

Main

A20, also referred to as Tumor Necrosis Factor alpha-induced protein 3 (TNFAIP3), has been implicated in diverse inflammatory diseases, and has been shown to act by repressing inflammatory NF-κB signaling and by promoting cell survival [1,2]. A20 is thought to act as a 'ubiquitin-editing' enzyme that inhibits NF-κB signaling by modulating the ubiquitination status of specific signaling proteins through the combined action of its deubiquitinase (DUB) activity and its E3 ubiquitin ligase activity that promotes K48-linked polyubiquitination and proteasomal degradation of its targets following tumor necrosis factor receptor 1 (TNFR1) activation [3]. However, transgenic mouse strains with inactivating mutations in A20's DUB or E3 ligase domains are grossly normal and do not develop spontaneous disease [4-6], in sharp contrast to the systemic inflammatory and perinatal lethality seen in A20-deficient mice [7]. These studies challenged the notion that A20 primarily acts via a 'ubiquitin editing' mechanism to suppress inflammation *in vivo*. Other studies suggest that the 7th zinc finger domain of A20 competes with the IκB kinase (IKK) adaptor protein NEMO for binding to linear (M1) ubiquitin chains generated by the linear ubiquitin chain assembly complex (LUBAC) to repress TNF-induced NF-κB signaling *in vitro* [8-10]. However, the physiological role of A20's ZnF7 domain is not known.

To determine the physiological role of the ZnF7 domain of A20 *in vivo*, we generated *Tnfaip3* gene-targeted A20 mutant mice carrying two cysteine to alanine point mutations in the ZnF7 motif - C764A and C767A (hereafter referred to as $A20^{ZnF7}$) (Extended Data Fig. 1a), which was previously shown to abrogate A20's ability to bind to linear polyubiquitin chains [8,10,11]. Homozygous $A20^{ZnF7/ZnF7}$ knock-in mice, derived from interbred $A20^{ZnF7/+}$ mice, were born with expected Mendelian frequency and did not display perinatal lethality (Extended Data Fig. 1b). This phenotype contrasts markedly with *Tnfaip3*$^{-/-}$ mice that, in our mouse facility, develop perinatal cachexia and die before weaning age (data not shown). However, all $A20^{ZnF7/ZnF7}$ knock-in mice had severely reduced body weight (Fig. 1a, Extended Data Fig. 1c) and only rarely produced offspring. Macroscopic and histological examination of young $A20^{ZnF7/ZnF7}$ mice revealed splenomegaly and lymphadenopathy (Extended Data Fig. 1d), paw swelling with absence of nails (Extended Data Fig. 1e), bone erosion (Extended Data Fig. 1f) and joint inflammation (Extended Data Fig. 1g), as previously shown [11], but also inflammation and immune cell infiltration in other tissues such as in the liver (Fig. 1b). Staining for cleaved caspase-3 revealed the presence of numerous apoptotic cells in $A20^{ZnF7/ZnF7}$ livers but not in control livers (Fig. 1c, d), suggesting that $A20^{ZnF7}$ expression sensitized hepatocytes to apoptosis. In agreement with the observed phenotype, $A20^{ZnF7/ZnF7}$ knock-in mice had high serum concentrations of the inflammatory

cytokines TNF and interleukin 6 (IL-6, Fig. 1e). Flow cytometric analyses of spleen tissue from 20 week-old mice revealed that $A20^{ZnF7/ZnF7}$ knock-in mice had increased numbers of myeloid cells but reduced numbers of B cells, T cells and natural killer (NK) cells, demonstrating that A20's ZnF7 domain regulates immune homeostasis (Fig. 1f, Extended Data Fig. 2). Finally, in agreement with the increased TNF concentrations detected in their serum, $A20^{ZnF7/ZnF7}$ myeloid cells displayed enhanced amounts of intracellular TNF (Fig. 1g).

Cachexia and premature lethality in A20-deficient mice were shown to be promoted by MyD88-mediated pro-inflammatory responses in the absence of A20 [12]. To address the role of MyD88-dependent signaling in the inflammatory pathology of $A20^{ZnF7/ZnF7}$ mice, these mice were crossed with *Myd88*$^{-/-}$ animals. As described recently [11], deletion of *Myd88* in $A20^{ZnF7/ZnF7}$ mice partly restored body weight (Extended Data Fig. 3a, b) and $A20^{ZnF7/ZnF7}$ *Myd88*$^{-/-}$ mice were partially protected from developing spontaneous tissue inflammation, as shown by reduced inflammation in liver (Extended Data Fig. 3c) and absence of swollen toes and ankles (Extended Data Fig. 3d). Inflammatory cytokine concentrations in serum of $A20^{ZnF7/ZnF7}$*Myd88*$^{-/-}$ mice were, however, elevated compared to control animals (Extended Data Fig. 3e). Together, these data demonstrate that MyD88-dependent mechanisms contribute to the local inflammatory pathology in the absence of ZnF7-dependent A20 functions, while more systemic inflammation is unaffected.

The role of A20 ZnF7 in regulating inflammation was further evaluated by examining the sensitivity of $A20^{ZnF7/ZnF7}$ mice to TNF *in vivo*. Indeed, an important anti-inflammatory and cytoprotective role for A20 has been demonstrated in intestinal epithelial cells (IECs), and IEC-specific A20-deficient mice ($A20^{IEC\text{-}KO}$) were previously shown to die from a challenge with a normally sublethal dose of TNF [13]. In contrast to the control mice, which all survived and only showed a modest drop in body temperature in the first hours after TNF injection, $A20^{ZnF7/ZnF7}$ mice displayed typical symptoms associated with TNF toxicity, including hypothermia and severe diarrhea, and all died within 3 h after TNF injection (Fig. 1h). $A20^{ZnF7/ZnF7}$ mice displayed severe damage of the small intestine, showing extensive epithelial destruction and presence of numerous cleaved caspase-3 positive apoptotic IECs, in contrast to control littermates which maintained tissue integrity without showing epithelial cell apoptosis. Next to the damage of the intestinal tissue, massive apoptosis could be detected in liver tissue of $A20^{ZnF7/ZnF7}$ mice upon exposure to TNF (Fig. 1i). Together, these data establish that A20's ZnF7 motif is essential to restrict inflammatory responses *in vivo*.

Consistent with the essential role of A20 as a negative feedback regulator of inducible NF-κB–dependent gene expression, cultured mouse embryonic fibroblasts (MEFs) from $A20^{ZnF7/ZnF7}$ knock-in

mice demonstrated increased TNF-induced NF-κB signaling, as reflected by earlier phosphorylation and sustained degradation of the NF-κB inhibitory molecule IκBα, and enhanced IL-6 production upon TNF stimulation compared to wild-type MEFs (Fig. 2a, b). Also cultured bone marrow-derived macrophages (BMDMs) from $A20^{ZnF7/ZnF7}$ knock-in mice showed sustained degradation of IκBα and expressed and produced increased amounts of cytokines than control BMDMs in response to lipopolysaccharide (LPS) and TNF (Fig. 2c,d, Extended Data Fig. 4). In agreement with the reported role of A20 ZnF7 in binding M1 ubiquitin chains[8-10], A20 recruitment to the TNFR1 complex was severely impaired upon stimulation of $A20^{ZnF7/ZnF7}$ BMDMs with Flag-tagged TNF, similar to what is observed in A20-deficient BMDMs (Fig. 2e). Absence of A20 at the membrane-bound signaling complex (known as complex I) was also associated with reduced abundance of M1 chains in the TNFR1 signaling complex I (Fig. 2f), which is consistent with the reported role of A20 recruitment in protecting M1 chains from degradation[9,14]. Mutation of ZnF7 did not prevent the recruitment of RIPK1 and TRADD adaptor proteins to the TNFR1 complex (Fig. 2f). Destabilization of complex I by reduced M1 ubiquitination favored formation of the death-inducing complex II and activation of an apoptotic caspase cascade (Fig. 2g, h), as previously reported[9,14].

We previously demonstrated that mice with a myeloid-restricted deficiency in A20 spontaneously develop polyarthritis caused by myeloid cell necroptosis, NLRP3 inflammasome hyperactivation and IL-1 receptor (IL-1R) signaling [11,15,16]. In agreement, $A20^{ZnF7/ZnF7}$ BMDMs showed significantly enhanced NLRP3 inflammasome-mediated caspase-1 activation, pyroptosis and IL-1β and IL-18 secretion upon stimulation with LPS and ATP (Fig. 2i-k). Together, these data illustrate the importance of the ZnF7 domain of A20 for preserving TNFR1 receptor complex integrity, and preventing cell death, inflammasome activation and inflammation.

Although $A20^{ZnF7/ZnF7}$ mice develop a spontaneous inflammatory phenotype, they do not fully recapitulate the phenotype of *Tnfaip3*$^{-/-}$ mice that develop severe multi-organ inflammation and cachexia and die in the first weeks after birth. This observation suggests that A20 exerts additional protective functions independent of its ZnF7 linear ubiquitin binding activity. In this respect, the ZnF4 domain of A20 has been demonstrated to bind K63-linked polyubiquitin, and mutations in the A20 ZnF4 ubiquitin-binding interface were shown to result in slightly impaired regulation of NF-κB signaling [4,17]. Gene-targeted mice mutated in the A20 ZnF4 domain, however, did not develop spontaneous pathology[4,6]. To clarify the physiological role of A20's ZnF4 domain in suppressing inflammation, we introduced two cysteine to alanine point mutations in the ZnF4 motif – C609A and C612A – of $A20^{ZnF7}$ mice, generating mice with combined inactivation of the K63 polyubiquitin binding ZnF4 and M1 polyubiquitin binding ZnF7 domains (hereafter referred to as $A20^{ZnF4ZnF7}$ mice)

(Extended Data Fig. 5a). Heterozygous A20$^{ZnF4ZnF7/+}$ mice had a normal appearance without evidence of clinical pathology. In contrast, although A20$^{ZnF4ZnF7/ZnF4ZnF7}$ mice were born at normal frequencies, they were severely runted and none of these animals survived past weaning age (Table 1, Extended data Fig. 5b). Gross and histological examination of tissues of 2-week-old A20$^{ZnF4ZnF7/ZnF4ZnF7}$ mice revealed severe inflammation in multiple organs, including intestine, liver, and skin (Fig. 3a, b), and cleaved caspase 3-positive cells were detected in livers of A20$^{ZnF4ZnF7/ZnF4ZnF7}$ mice, indicative of spontaneous liver cell apoptosis (Fig. 3c, d). In addition, systemic inflammation in A20$^{ZnF4ZnF7/ZnF4ZnF7}$ mice was also evident from the detection of high serum concentrations of the inflammatory cytokines TNF and IL-6 (Fig. 3e).

A20$^{ZnF4ZnF7/ZnF4ZnF7}$ mice in a MyD88-deficient background did not die in the first postnatal weeks as is the case with A20$^{ZnF4ZnF7/ZnF4ZnF7}$ mice (Extended Data Fig. 5c) and did not develop the severe tissue pathology as seen in MyD88-sufficient controls (Fig. 3f). However, these mice still failed to thrive, presented with severely reduced bodyweight and did not survive beyond 20 weeks of age (Fig 3g). Although 15 week-old A20$^{ZnF4ZnF7/ZnF4ZnF7}$*Myd88*$^{-/-}$ did not display pronounced swelling of ankles and toes (Fig. 3h), histological examination still revealed inflammation in liver tissue of these mice (Fig. 3i). These results demonstrate that MyD88 drives dysregulated homeostatic TLR signals in the absence of ZnF4 and ZnF7-dependent A20 functions in young mice, whereas MyD88-independent inflammatory signaling contributed to pathology at older age.

Because A20$^{ZnF4ZnF7/ZnF4ZnF7}$ mice are not viable, we next developed mice with a conditional 'floxed' allele of *Tnfaip3*, allowing tissue-specific expression of the ZnF4 and ZnF7 mutations through expression of a Cre recombinase (Extended data Fig. 6a). Mice homozygous for the loxP-flanked *Tnfaip3*^{ZnF4ZnF7} allele expressed normal amounts of A20 and developed normally (data not shown). General deletion of the loxP-flanked *Tnfaip3*^{ZnF4ZnF7} alleles through expression of a ubiquitous Cre recombinase triggered severe pathology and postnatal lethality, reminiscent of our observations in A20$^{ZnF4ZnF7/ZnF4ZnF7}$ mice (Fig. 4a and Extended Data Fig. 6b). To test if myeloid-specific *Tnfaip3*$^{ZnF4ZnF7/ZnF4ZnF7}$ mice (*Tnfaip3*$^{ZnF4ZnF7/ZnF4ZnF7}$*LysM*-Cre) also developed spontaneous arthritis as seen in myeloid-specific A20-deficient mice [11,15,16], we crossed loxP-flanked *Tnfaip3*^{ZnF4ZnF7} mice with *LysM*-Cre mice. Indeed, *Tnfaip3*$^{ZnF4ZnF7/ZnF4ZnF7}$*LysM*-Cre mice developed a progressive polyarthritis, characterized by immune cell infiltration, cartilage destruction indicated by decreased proteoglycan staining with toluidine blue, and bone erosion with increased osteoclast activity detected by tartrate-resistant acid phosphatase (TRAP) staining (Fig. 4b-e and Extended Data Fig. 6c). Myeloid-specific *Tnfaip3*$^{ZnF4ZnF7/ZnF4ZnF7}$ mice also had significantly higher serum concentrations of the inflammatory cytokines TNF and IL-6 compared to control littermate mice (Fig. 4f). In line with these *in vivo*

observations, cultured BMDMs from *Tnfaip3*$^{ZnF4ZnF7/ZnF4ZnF7}$*LysM*-Cre mice produced significantly more cytokines upon stimulation with LPS compared to control BMDMs (Fig. 4g), consistent with the role of A20 as a negative feedback regulator of inducible NF-κB–dependent gene expression.

To investigate the consequence of mutant A20^{ZnF4ZnF7} expression in intestinal epithelial cells (IECs), we generated IEC-specific *Tnfaip3*$^{ZnF4ZnF7/ZnF4ZnF7}$ mice by crossing loxP-flanked *Tnfaip3*^{ZnF4ZnF7} mice with villin-Cre mice (*Tnfaip3*$^{ZnF4ZnF7/ZnF4ZnF7}$*Vil1*-Cre), and challenged these animals with a normally sublethal dose of TNF. As expected, control littermates all survived and only showed a modest drop in body temperature. In contrast, and as previously demonstrated in IEC-specific A20-deficient mice [13], IEC-specific *Tnfaip3*$^{ZnF4ZnF7/ZnF4ZnF7}$ mice displayed typical symptoms associated with TNF toxicity, including hypothermia and severe diarrhea, and all died between 5 and 10 h after injection due to the TNF-induced apoptosis of A20 mutant IECs (Fig. 4h-j). Finally, IEC-specific *Tnfaip3*$^{ZnF4ZnF7/ZnF4ZnF7}$ mice and control littermates were evaluated in the model of dextran sodium sulfate (DSS)-induced colitis. Mice were subjected to 1.5 % DSS in drinking water for 5 days and monitored daily for clinical pathology. Compared with control mice, IEC-*Tnfaip3*$^{ZnF4ZnF7/ZnF4ZnF7}$ mice showed increased susceptibility to DSS-induced colitis, similar to what had been shown with IEC-specific A20-deficient mice [13] (Extended Data Fig. 6d). In agreement, IEC-*Tnfaip3*$^{ZnF4ZnF7/ZnF4ZnF7}$ mice showed more pronounced loss of intestinal barrier integrity after 5 days of DSS compared to the control group (Extended Data Fig. 6e). Unchallenged mice, however, did no show spontaneous barrier permeability (Extended Data Fig. 6e).

In conclusion, we have demonstrated that A20 acts primarily as an ubiquitin-binding protein via both its ZnF4 and ZnF7 domains to suppress pro-inflammatory signaling. Upon TNFR1 and TLR4 activation, A20 is recruited to the receptor complexes through binding to linear ubiquitin chains via its ZnF7 in order to stabilize the respective signaling complexes and dampen downstream inflammatory signaling. We further show that A20's anti-inflammatory activity also relies on its K63 ubiquitin-binding ZnF4 domain, and mice lacking both functional ZnF4 and ZnF7 domains phenocopy A20-deficient mice in that they die perinatally due to severe multi organ inflammation. Together, our observations suggest a mainly non-enzymatic role for A20 in suppressing inflammation by allowing its recruitment and the stabilization of ubiquitin chains in the receptor complex. However, A20's DUB function may still be important in the downstream regulation of signaling. More studies, however, are needed to further investigate this.

Multiple genetic studies over the past ten years have associated *TNFAIP3* polymorphisms to diverse human inflammatory and autoimmune diseases[2]. These disease-associated variants are mostly located in upstream or downstream non-coding regions or in intronic regions of the *TNFAIP3* gene,

199 which may affect the expression of A20 possibly by interfering with the function of cell- and
200 activation-specific enhancers [18-21]. Also loss-of-function mutations and deletions in *TNFAIP3* have
201 been identified, especially in patients with B cell lymphomas [22-24]. The majority of these *TNFAIP3*
202 mutations concern frameshift and premature stop codon mutations preventing the synthesis or
203 compromising the ubiquitin-binding ability of the C-terminal ZnF7 domain [8,22-24]. Furthermore, A20
204 haploinsufficiency has recently been shown to cause a severe early-onset autoinflammatory disease,
205 and peripheral blood monocytes isolated from these patients show severely reduced A20 expression
206 [25]. Our findings presented here suggest that these mutations may cause a polyubiquitin-binding
207 defect, that in these patients may be sufficient to affect homeostatic regulation of NF-κB signaling
208 and cell death.

209

ACKNOWLEDGEMENTS

We thank D. Huyghebaert, L. Bellen and D. Vanhede for animal care and A. Fossoul and M. Gennadi for excellent technical assistance. We also thank the InfrafrontierGR infrastructure (ERDF and NSRF 2007-2013 and 2014-2020) for providing histology and mCT facilities. A. Martens is supported by a grant from the "Concerted Research Actions" (GOA) of the Ghent University. Research in the G. van Loo lab is supported by research grants from the FWO, the "Geneeskundige Stichting Koningin Elisabeth" (GSKE), the CBC Banque Prize, the Charcot Foundation, the "Belgian Foundation against Cancer", "Kom op tegen Kanker", and the GOA of the Ghent University. M.A. lab is supported by a startup grant from the Stavros Niarchos Foundation donation to BSRC "Al. Fleming.

COMPETING FINANCIAL INTERESTS

M.L. is an employee of Janssen Pharmaceutica. All authors declare that they have no conflict of interest.

AUTHOR CONTRIBUTIONS

A.M., D.P., E.H., J.V., S.R., L.C., S.V., L.D., M.S., H.V., K.S., T.H. and K.I. performed the experiments. A.M., D.P., E.H., J.V., L.C., S.V., A.W., S.J., M.L., R.B., M.A., M.J.M.B. and G.v.L. analyzed the data. G.v.L. provided ideas and coordinated the project. A.M. and G.v.L. wrote the manuscript.

References

1 Catrysse, L., Vereecke, L., Beyaert, R. & van Loo, G. A20 in inflammation and autoimmunity. *Trends Immunol* **35**, 22-31, doi:10.1016/j.it.2013.10.005 (2014).

2 Martens, A. & van Loo, G. A20 at the Crossroads of Cell Death, Inflammation, and Autoimmunity. *Cold Spring Harbor perspectives in biology*, doi:10.1101/cshperspect.a036418 (2019).

3 Wertz, I. E. *et al.* De-ubiquitination and ubiquitin ligase domains of A20 downregulate NF-kappaB signalling. *Nature* **430**, 694-699 (2004).

4 Lu, T. T. *et al.* Dimerization and ubiquitin mediated recruitment of A20, a complex deubiquitinating enzyme. *Immunity* **38**, 896-905, doi:10.1016/j.immuni.2013.03.008 (2013).

5 De, A., Dainichi, T., Rathinam, C. V. & Ghosh, S. The deubiquitinase activity of A20 is dispensable for NF-kappaB signaling. *EMBO Rep* **15**, 775-783, doi:10.15252/embr.201338305 (2014).

6 Wertz, I. E. *et al.* Phosphorylation and linear ubiquitin direct A20 inhibition of inflammation. *Nature* **528**, 370-375, doi:10.1038/nature16165 (2015).

7 Lee, E. G. *et al.* Failure to regulate TNF-induced NF-kappaB and cell death responses in A20-deficient mice. *Science* **289**, 2350-2354 (2000).

8 Tokunaga, F. *et al.* Specific recognition of linear polyubiquitin by A20 zinc finger 7 is involved in NF-kappaB regulation. *EMBO J* **31**, 3856-3870, doi:10.1038/emboj.2012.241 (2012).

9 Draber, P. *et al.* LUBAC-Recruited CYLD and A20 Regulate Gene Activation and Cell Death by Exerting Opposing Effects on Linear Ubiquitin in Signaling Complexes. *Cell reports* **13**, 2258-2272, doi:10.1016/j.celrep.2015.11.009 (2015).

10 Verhelst, K. *et al.* A20 inhibits LUBAC-mediated NF-kappaB activation by binding linear polyubiquitin chains via its zinc finger 7. *EMBO J* **31**, 3845-3855, doi:10.1038/emboj.2012.240 (2012).

11 Polykratis, A. *et al.* A20 prevents inflammasome-dependent arthritis by inhibiting macrophage necroptosis through its ZnF7 ubiquitin-binding domain. *Nature cell biology* **21**, 731-742, doi:10.1038/s41556-019-0324-3 (2019).

12 Turer, E. E. *et al.* Homeostatic MyD88-dependent signals cause lethal inflamMation in the absence of A20. *J Exp Med* **205**, 451-464, doi:10.1084/jem.20071108 (2008).

13 Vereecke, L. *et al.* Enterocyte-specific A20 deficiency sensitizes to tumor necrosis factor-induced toxicity and experimental colitis. *The Journal of experimental medicine* **207**, 1513-1523, doi:10.1084/jem.20092474 (2010).

14 Priem, D. *et al.* A20 protects cells from TNF-induced apoptosis through linear ubiquitin-dependent and -independent mechanisms. *Cell death & disease* **10**, 692, doi:10.1038/s41419-019-1937-y (2019).

15 Matmati, M. *et al.* A20 (TNFAIP3) deficiency in myeloid cells triggers erosive polyarthritis resembling rheumatoid arthritis. *Nature genetics* **43**, 908-912, doi:10.1038/ng.874 (2011).

16 Vande Walle, L. *et al.* Negative regulation of the NLRP3 inflammasome by A20 protects against arthritis. *Nature* **512**, 69-73, doi:10.1038/nature13322 (2014).

17 Bosanac, I. *et al.* Ubiquitin binding to A20 ZnF4 is required for modulation of NF-kappaB signaling. *Mol Cell* **40**, 548-557, doi:10.1016/j.molcel.2010.10.009 (2010).

18 Graham, R. R. *et al.* Genetic variants near TNFAIP3 on 6q23 are associated with systemic lupus erythematosus. *Nat Genet* **40**, 1059-1061, doi:10.1038/ng.200 (2008).

19 Adrianto, I. *et al.* Association of a functional variant downstream of TNFAIP3 with systemic lupus erythematosus. *Nature genetics* **43**, 253-258, doi:10.1038/ng.766 (2011).

20 Sokhi, U. K. *et al.* Dissection and function of autoimmunity-associated TNFAIP3 (A20) gene enhancers in humanized mouse models. *Nat Commun* **9**, 658, doi:10.1038/s41467-018-03081-7 (2018).
21 Wang, S., Wen, F., Wiley, G. B., Kinter, M. T. & Gaffney, P. M. An enhancer element harboring variants associated with systemic lupus erythematosus engages the TNFAIP3 promoter to influence A20 expression. *PLoS Genet* **9**, e1003750, doi:10.1371/journal.pgen.1003750 (2013).
22 Compagno, M. *et al.* Mutations of multiple genes cause deregulation of NF-kappaB in diffuse large B-cell lymphoma. *Nature* **459**, 717-721, doi:10.1038/nature07968 (2009).
23 Kato, M. *et al.* Frequent inactivation of A20 in B-cell lymphomas. *Nature* **459**, 712-716, doi:10.1038/nature07969 (2009).
24 Schmitz, R. *et al.* TNFAIP3 (A20) is a tumor suppressor gene in Hodgkin lymphoma and primary mediastinal B cell lymphoma. *J Exp Med* **206**, 981-989, doi:10.1084/jem.20090528 (2009).
25 Zhou, Q. *et al.* Loss-of-function mutations in TNFAIP3 leading to A20 haploinsufficiency cause an early-onset autoinflammatory disease. *Nat Genet* **48**, 67-73, doi:10.1038/ng.3459 (2016).

Figure legends

Figure 1. $A20^{ZnF7/ZnF7}$ knock-in mice develop spontaneous inflammatory pathology and are sensitized to TNF induced toxicity. (a) Bodyweight of $A20^{ZnF7/+}$ and $A20^{ZnF7/ZnF7}$ mice in function of time. Each dot represents a biologically independent mouse (9 week-old mice: $A20^{ZnF7/+}$, n=16; $A20^{ZnF7/ZnF7}$, n=6; 12 week-old mice: $A20^{ZnF7/+}$, n=15; $A20^{ZnF7/ZnF7}$, n=7; 15week-old mice: $A20^{ZnF7/+}$, n=11; $A20^{ZnF7/ZnF7}$, n=7). Data are expressed as mean ± SEM. **** represents p<0.0001 (parametric two-way ANOVA between indicated genotypes). **(b)** Representative hematoxylin-eosin-stained sections of liver from 28-week-old control ($A20^{+/+}$) and $A20^{ZnF7/ZnF7}$ littermates. Scale bar, 200 µm and 50 µm (insert). Picture representative for at least 5 biologically independent mice per group. **(c-d)** Immunohistochemistry for cleaved caspase 3 on liver sections from $A20^{ZnF7/ZnF7}$ mice and control ($A20^{+/+}$) littermates (c), and number of cleaved caspase 3-positive cells per mm^2 ($A20^{ZnF7/ZnF7}$, n=5 biologically independent samples; $A20^{+/+}$, n=4 biologically independent samples) (d). Pictures shown are representative for 5 biologically independent mice per group. Scale bar, 20 µm (insert, 10 µm) Data are expressed as mean ± SEM. * represents p=0.0159 (Two-sided non-parametric Mann Whitney test between indicated genotypes). **(e)** Levels of IL-6 and TNF in serum of control ($A20^{+/+}$), $A20^{ZnF7/+}$ and $A20^{ZnF7/ZnF7}$ mice at the age between 15 and 30 weeks. Each dot represents a biologically independent mouse (IL-6: $A20^{+/+}$, n=16; $A20^{ZnF7/+}$, n=14; $A20^{ZnF7/ZnF7}$, n=25; TNF: $A20^{+/+}$, n=11; $A20^{ZnF7/+}$, n=4; $A20^{ZnF7/ZnF7}$, n=20). Data are expressed as mean ± SEM. *, ** and **** represent p=0.0133, p=0.0014 and p<0.0001 respectively (parametric one-way ANOVA between indicated genotypes). **(f)** Absolute cell numbers of indicated immune cell populations in the spleens of $A20^{+/+}$, $A20^{ZnF7/+}$ and $A20^{ZnF7/ZnF7}$ mice, as measured by flow cytometry. Each dot represents a biologically independent mouse ($A20^{+/+}$, n=6; $A20^{ZnF7/+}$, n=6; $A20^{ZnF7/ZnF7}$, n=8). Data are expressed as mean ± SEM. *, **, *** represents $p < 0.05$, $p < 0.01$ and $p < 0.001$ (Two-sided non-parametric Mann-Whitney test between indicated genotypes). **(g)** Splenocytes isolated from $A20^{+/+}$, $A20^{ZnF7/+}$ and $A20^{ZnF7/ZnF7}$ mice were incubated for 4 hours in the presence of protein transport inhibitors to assess intracellular TNF production by flow cytometry. Bar graphs represent percentage TNF that is produced within total macrophage (top) and $Ly6C^{hi}$ monocyte (bottom) populations. Each dot represents a biologically independent mouse ($A20^{+/+}$, n=5; $A20^{ZnF7/+}$, n=4; $A20^{ZnF7/ZnF7}$, n=5). Data are expressed as mean ± SEM. * and ** represent $p < 0.05$ and $p < 0.01$ respectively (Two-sided non-parametric Mann-Whitney test between indicated genotypes). **(h)** Body temperature and survival of $A20^{ZnF7/ZnF7}$ mice and control littermates injected with recombinant mTNF (i.p., 5 µg / 20 g of bodyweight), in function of time ($A20^{+/+}$, n=7; $A20^{ZnF7/+}$, n=5; $A20^{ZnF7/ZnF7}$, n=5 mice). Data are expressed as mean ± SEM. p < ** and *** represent p<0.01, p<0.001, respectively (body temperature, REML analysis and survival, two-sided

mantel-cox test). **(i)** Cleaved caspase 3 staining on sections from small intestine (SI) and liver from control ($A20^{+/+}$) and $A20^{ZnF7/ZnF7}$ mice. Scale bar, 200 µm (liver) and 100 µm (SI). Pictures shown are representative for 5 biologically independent mice per group.

Figure 2. ZnF7 is critical for A20-mediated suppression of inflammatory signaling and cell death. (a) Western blot analysis of whole cell lysates from $A20^{+/+}$, $A20^{ZnF7/ZnF7}$ and $A20^{-/-}$ MEF cells stimulated with TNF for the indicated time periods**.** Actin is shown as a loading control. Figure representative for 3 independent experiments. **(b)** IL-6 secretion by control $A20^{+/+}$, $A20^{ZnF7/ZnF7}$ and $A20^{-/-}$ MEF cells, either or not stimulated with TNF for 4 h ($A20^{+/+}$, n=3; $A20^{ZnF7/ZnF7}$, n=3; $A20^{-/-}$, n=3 independent cell cultures). **** represents p<0.0001 (parametric two-way ANOVA between indicated genotypes). Data are expressed as mean ± SEM. **(c)** Western blot analysis of whole cell lysates from $A20^{+/+}$, $A20^{ZnF7/ZnF7}$ and $A20^{myel\text{-}KO}$ BMDMs stimulated with LPS as indicated**.** β-tubulin is shown as a loading control. Figure representative for 3 independent experiments. **(d)** TNF and IL-6 secretion by BMDMs isolated from control $A20^{+/+}$ (n=5), $A20^{ZnF7/ZnF7}$(n=5) and $A20^{myel\text{-}KO}$ (n=5) mice, either or not stimulated with LPS for 6 h. *** and **** represent p<0.001 and p<0.0001 respectively (parametric two-way ANOVA between indicated genotypes). Data are expressed as mean ± SEM. **(e)** TNFR1 pulldown assay in BMDMs isolated from $A20^{+/+}$, $A20^{myel\text{-}KO}$ and $A20^{ZnF7/ZnF7}$ mice after stimulation with Flag-TNF (1 µg/ml) for the indicated time periods, and immunoprecipitation of the TNFR1 complex with anti-Flag beads in presence of USP2 (24 µg/ml) and immunoblot for A20. Actin is shown as a loading control. Figure representative for 3 independent experiments. **(f)** TNFR1 pulldown on BMDMs isolated from $A20^{+/+}$, $A20^{myel\text{-}KO}$ and $A20^{ZnF7/ZnF7}$ mice stimulated with Flag-TNF (1 µg/ml) for the indicated time periods, and immunoprecipitation of the TNFR1 complex using anti-Flag beads and immunoblotted for A20, RIPK1, TRADD and M1. Figure representative for 3 independent experiments. **(g)** Cell death induction in $A20^{+/+}$, $A20^{ZnF7/ZnF7}$ and $A20^{-/-}$ MEFs stimulated with mouse TNF, in function of time as measured by SytoxGreen (SG+) positivity. Data are expressed as mean ± SEM, and representative of 3 independent experiments ($A20^{+/+}$, n=3; $A20^{ZnF7/ZnF7}$, n=3; $A20^{myel\text{-}KO}$, n=3 independent cell cultures). ** represents p<0.01 (RELM analysis) **(h)** Western blot analysis for expression of A20, full-length (FL) and cleaved (Cl) caspase-3 in $A20^{+/+}$, $A20^{ZnF7/ZnF7}$ and $A20^{-/-}$ MEFs stimulated with mouse TNF for the indicated time points. Actin is shown as loading control. Figure representative for 3 independent experiments **(i)** Immunoblot for procaspase-1 and cleaved caspase-1 (p20) in BMDMs from $A20^{+/+}$, $A20^{ZnF7/ZnF7}$ and $A20^{myel\text{-}KO}$ either or not stimulated with LPS and/or ATP. Actin is shown as loading control. Data are representative of three independent experiments. **(j)** IL1β and IL18 secretion by BMDMs isolated from $A20^{+/+}$ (n=5), $A20^{ZnF7/ZnF7}$ (n=5) and $A20^{myel\text{-}KO}$ (n=5) mice either or not stimulated

with LPS and ATP. Data represent the mean ± SEM.**, **** represent p<0.01 and p<0.0001, respectively (parametric two-way ANOVA between indicated genotypes). **(k)** Pyroptosis induction in BMDMs from $A20^{+/+}$ (n=5), $A20^{ZnF7/ZnF7}$ (n=5) and $A20^{myel\text{-}KO}$ (n=5) mice stimulated with LPS and ATP, as measured by Sytox Green (SG) uptake. Data are presented as mean ± SEM and are representative of three independent experiments. *** represents p<0.001 (RELM analysis).

Figure 3. $A20^{ZnF4ZnF7/ZnF4ZnF7}$ knock-in mice phenocopy A20 knockout mice. (a) Gross appearance of livers of 2-week old control $A20^{+/+}$, $A20^{ZnF4ZnF7/+}$ and $A20^{ZnF4ZnF7/ZnF4ZnF7}$ mice. Note pale acellular regions in $A20^{ZnF4ZnF7/ZnF4ZnF7}$ livers. Picture representative for 3 biologically independent mice. **(b)** Representative hematoxylin-eosin-stained sections from 2-week old control $A20^{+/+}$, $A20^{ZnF4ZnF7/+}$ and $A20^{ZnF4ZnF7/ZnF4ZnF7}$ intestine (small intestine and colon), liver and skin. Note severe inflammation in all $A20^{ZnF4ZnF7/ZnF4ZnF7}$ tissue sections. Scale bar, 100 µm. Pictures representative for 3 biologically independent mice. **(c)** Immunostaining for cleaved caspase 3 on liver sections from 2-week old control $A20^{+/+}$ and $A20^{ZnF4ZnF7/ZnF4ZnF7}$ mice. Pictures representative for 3 biologically independent mice. Scale bars, 50 µm (insert, 20 µm). **(d)** Quantification of cleaved caspase 3-positive cells in sections from the liver of 2-week old control $A20^{+/+}$and $A20^{ZnF4ZnF7/ZnF4ZnF7}$ mice. Number of cleaved caspase 3-positive cells per mm^2 is shown ($A20^{ZnF4ZnF7/ZnF4ZnF7}$, n= 5; $A20^{+/+}$, n=3 mice) Data are expressed as mean ± SEM. Each dot represents an individual mouse. *, p=0.036 (two-sided non-parametric Mann Whitney test between indicated genotypes). **(e)** Levels of IL-6 and TNF in serum of control $A20^{+/+}$, $A20^{ZnF4ZnF7/+}$ and $A20^{ZnF4ZnF7/ZnF4ZnF7}$ mice at the age of 2 weeks. Each dot represents a biologically independent mouse ($A20^{+/+}$, n=19; $A20^{ZnF4ZnF7/+}$, n=21; $A20^{ZnF4ZnF7/ZnF4ZnF7}$, n=11). Data are expressed as mean ± SEM. ****, p<0.0001 (parametric one-way ANOVA between indicated genotypes). **(f)** Representative hematoxylin-eosin-stained sections from liver and skin tissue of 2 week-old $A20^{ZnF4ZnF7/ZnF4ZnF7}MyD88^{-/-}$ mice and $A20^{ZnF4ZnF7/ZnF4ZnF7}MyD88^{+/-}$ littermates. Scale bar, 100 µm. Pictures representative for 3 biologically independent mice. **(g)** Bodyweight of 15-week old $A20^{ZnF4ZnF7/ZnF4ZnF7}MyD88^{-/-}$ mice compared to control mice. Data are expressed as mean ± SEM. Each dot represents a biologically independent mouse ($A20^{ZnF4ZnF7/+}MyD88^{+/+}$, n=5; $A20^{+/+}MyD88^{-/-}$, n=11; $A20^{ZnF4ZnF7/ZnF4ZnF7}MyD88^{-/-}$, n=5). **** represents p<0.0001 (parametric one-way ANOVA between indicated genotypes). **(h)** Representative pictures of hindpaws of 15 week-old $A20^{ZnF4ZnF7/ZnF4ZnF7}MyD88^{-/-}$ mice and control wild-type mice. **(i)** Representative hematoxylin-eosin-stained liver sections from 15 week-old $A20^{ZnF4ZnF7/ZnF4ZnF7}MyD88^{-/-}$ mice and control wild-type mice (scale bars, 50µm). Pictures representative for 3 biologically independent mice. Mark that

A20$^{ZnF4ZnF7/ZnF4ZnF7}$ could not be used as control mice in Fig. 3g-i since these mice do not survive beyond the age of 3 weeks.

Figure 4. Tissue-specific A20^{ZnF4ZnF7} expression phenocopies tissue-specific A20 deficiency. (a) Gross appearance of livers of 2-week old control (*Tnfaip3*$^{ZnF4ZnF7/ZnF4ZnF7}$CreDel$^{+/+}$) and *Tnfaip3*$^{ZnF4ZnF7/ZnF4ZnF7}$CreDel$^{Tg/+}$ littermate mice. Note pale acellular regions in *Tnfaip3*$^{ZnF4ZnF7/ZnF4ZnF7}$CreDel$^{Tg/+}$ livers. **(b)** Representative picture of the hind paws of 32 week-old control (*Tnfaip3*$^{ZnF4ZnF7/ZnF4ZnF7}$LysMCre$^{+/+}$) and *Tnfaip3*$^{ZnF4ZnF7/ZnF4ZnF7}$LysMCre$^{Tg/+}$ littermate mice. **(c)** Biweekly clinical arthritis scores of the ankles of control (*Tnfaip3*$^{ZnF4ZnF7/ZnF4ZnF7}$LysMCre$^{+/+}$) and *Tnfaip3*$^{ZnF4ZnF7/ZnF4ZnF7}$LysMCre$^{Tg/+}$ littermate mice (*Tnfaip3*$^{ZnF4ZnF7/ZnF4ZnF7}$LysMCre$^{+/+}$, n=6-15 mice per age, *Tnfaip3*$^{ZnF4ZnF7/ZnF4ZnF7}$LysMCre$^{Tg/+}$, n=12-25 mice per age). Data are expressed as mean ± SEM. ** represents p=0.002 (REML analysis) **(d)** Histological images of H&E-stained ankle joints of mice with the indicated genotypes. Pictures representative for 5 biologicaly independent mice. **(e)** Graphs depicting histological scores for inflammation, bone erosion and cartilage destruction in mice with the indicated genotypes (28-33 weeks). Dots in the graphs indicate individual mice (*Tnfaip3*$^{ZnF4ZnF7/ZnF4ZnF7}$LysMCre$^{+/+}$, n=10; *Tnfaip3*$^{ZnF4ZnF7/ZnF4ZnF7}$LysMCre$^{Tg/+}$, n=21). Data are expressed as mean ± SEM. *, *** and **** represent p=0.0141, p=0.0003 and p<0.0001 respectively (Two-sided non-parametric Mann-Whitney test between indicated genotypes). **(f)** Levels of IL-6 and TNF in serum of control (*Tnfaip3*$^{ZnF4ZnF7/ZnF4ZnF7}$LysMCre$^{+/+}$) and *Tnfaip3*$^{ZnF4ZnF7/ZnF4ZnF7}$LysMCre$^{Tg/+}$ mice at the age of 30-40 weeks. Each dot represents a biologically independent mouse (*Tnfaip3*$^{ZnF4ZnF7/ZnF4ZnF7}$LysMCre$^{+/+}$, n=11, *Tnfaip3*$^{ZnF4ZnF7/ZnF4ZnF7}$LysMCre$^{Tg/+}$, n=27). Data are expressed as mean ± SEM. ** and **** represent p=0.0017 and p<0.0001 respectively (Two-sided non-parametric Mann-Whitney test between indicated genotypes). **(g)** TNF and IL-6 secretion by BMDMs isolated from control (*Tnfaip3*$^{ZnF4ZnF7/ZnF4ZnF7}$LysMCre$^{+/+}$**,** n=6), *Tnfaip3*$^{ZnF4ZnF7/ZnF4ZnF7}$LysMCre$^{Tg/+}$ (n=6) and A20$^{myel\text{-}KO}$ (n=6) littermate mice stimulated with LPS for the indicated time points. Data are expressed as mean ± SEM. **, *** and **** represent p<0.01, p<0.001 and p<0.0001 respectively (parametric two-way ANOVA between indicated genotypes at each time point). **(h-j)** *Tnfaip3*$^{ZnF4ZnF7/ZnF4ZnF7}$villinCre$^{Tg/+}$ (n=5) and control (*Tnfaip3*$^{ZnF4ZnF7/ZnF4ZnF7}$villinCre$^{+/+}$**,** n=6) littermate mice were injected i.p. with 5 µg recombinant mouse TNF per 20 g of bodyweight. Body temperature (h, mean ± SEM, *** represents p<0.001, REML analysis) and survival (i, ** represents p=0.0018, Two-sided mantel-cox test) in function of time. **(j)** Representative cleaved caspase 3-specific staining on sections of small intestine of mice with the indicated genotypes 5 h past TNF injection. Scale bar, 100µm.

Tables

Table 1 : Birth and survival rates of control $A20^{+/+}$, $A20^{ZnF4ZnF7/+}$ and $A20^{ZnF4ZnF7/ZnF4ZnF7}$ offspring from $A20^{ZnF4ZnF7/+}$ x $A20^{ZnF4ZnF7/+}$ breeding couples.

Genotype	Expected	Observed (at birth)	Observed (at weaning)
$A20^{+/+}$	25 % (20)	18	18
$A20^{ZnF4ZnF7/+}$	50 % (40)	46	46
$A20^{ZnF4ZnF7/ZnF4ZnF7}$	25 % (20)	16	0
Total (observed)	100 % (52)	52	64

Methods

***Mice*.** For the generation of gene-targeted A20-ZnF7 mice, Cas9 mRNA (Sigma) and protein (VIB Protein Service Facility, Ghent) together with a 151 bp single-stranded repair template (IDT) containing the homologous sequence around the mutations and two short guide RNAs (sgRNAs, Synthego) targeting the ZnF7 domain of the murine *Tnfaip3* gene were microinjected into the pronucleus of zygotes obtained from C57BL/6J mice. Embryos were overnight incubated in KSOM medium and transferred the next day to foster mothers via oviduct transfer. sgRNA1: 5'-AGCCATACATCTGCTTGAACTGG-3'; sgRNA2: 5'-ATTGCAGTAACCATTACACTTGG-3'; ssDNA oligonucleotides used as repair template containing two Cys-to-Ala point-mutations [TGC>GCC (C764A); TGC>GCT (C767A)] and two silent mutations [GCC>GCT (A758); TAC>TAT (Y768)] to avoid re-editing after recombination: 5'-GCCTGAAGAGCCCCCTAAACAGCGCTGCCGGGCCCCTGCTTGTGATCACTTTGGCAATGCTAAGTGTAATGGT TACGCCAATGAGGCTTATCAGTTCAAGCAGATGTATGGCTAAGTGCGAACACATTGACAGGTCCAGCAAGAAG GAGCC-3'. For the generation of A20-ZnF4/ZnF7 knockin mice, Cas9 protein together with a donor vector containing ~1 kb 5' and 3' homologous arms around the Cys-to-Ala mutations [TGC>GCC (C609A); TGT>GCT (C612A); TGC>GCC (C764A); TGC>GCC (C767A)] and two synonymous mutations [TCC>TCA (S577); TAC>TAT (Y768)], and two sgRNAs (sgRNA1: 5'- CTCCTGGAGTCCGTGCAGCCTGG-3'; sgRNA2: 5'-AGCCATACATCTGCTTGAACTGG-3') targeting the ZnF4 and ZnF7 domain of the murine A20 gene were microinjected into the pronucleus of zygotes obtained from C57BL/6 mice. Conditional LoxP-flanked A20-ZnF4/ZnF7 knockin alleles were generated through homologous recombination in C57BL/6 ES cells. A neomycin resistance cassette flanked with RoxP sites was introduced after the last exon (exon 9) of the *Tnfaip3* gene. Exons 6-9 and the neo cassette are flanked with LoxP sites. At the 3' of the loxP flanked region we introduced a mutated exon 6-9 containing the ZnF4 (C609A/C612A) and ZnF7 (C764A/C767A) mutations. In $Tnfaip3^{ZnF4ZnF7}$ floxed mice the neomycine cassette has been removed by Dre-mediated recombination. Cre-mediated recombination excises the LoxP-flanked fragment containing the wild-type exons 6-9, resulting in the expression of the mutated exons 6-9. Mice with conditional LoxP-flanked $Tnfaip3^{ZnF4ZnF7}$ alleles were crossed with the *LysM*-Cre[26] or *Vil1*-Cre transgenic lines[27]. $Myd88^{-/-}$ mice were previously described[28]. Mice were housed in individually ventilated cages at the VIB Center for Inflammation Research, in a specific pathogen-free animal facility. All experiments on mice were conducted

according to institutional, national and European animal regulations. Animal protocols were approved by the ethics committee of Ghent University.

Histological analysis of tissue sections. Liver, spleen, small intestine, colon, skin and joint sections were fixed in 4% paraformaldehyde for hematoxylin and eosin or immunostaining, or in Carnoy fixative (60% methanol, 30% chloroform, 10% glacial acetic acid) for Alcian Blue/Periodic Acid (AB/PAS) staining. Samples were dehydrated, embedded in paraffin, sectioned at 4 μm and examined by light microscopy. Bright-field microscopy was done using an Axio Scan.Z1 (Zeiss). For joint pathology, formalin-fixed, EDTA-decalcified, paraffin-embedded mouse tissue specimens were sectioned and stained with hematoxylin and eosin, Toluidine Blue and TRAP [Leukocyte Acid Phosphatase Kit; Sigma-Aldrich]. H&E-, Toluidine Blue- and TRAP-stained joint sections were semi-quantitatively and blindly evaluated for the following parameters: synovial inflammation/ hyperplasia (scale of 0–5), cartilage erosion (scale of 0–5), and bone loss (scale of 0–5) as described[29].

Isolation and immortalization of mouse embryonic fibroblasts. 12.5 dpc embryos from $A20^{ZnF7/+}$ or $A20^{ZnF4ZnF7/+}$ matings were isolated and mouse embryonic fibroblasts (MEFs) were prepared. MEFs were immortalized through serial passaging and frozen in liquid nitrogen. Confluent cells were stimulated with 20 ng/ml recombinant mouse TNF, after which cells were lysed for immunoblotting or quantitative real-time PCR.

Isolation of bone marrow-derived macrophages. BMDMs were obtained from bone marrow cells flushed from mouse femurs and tibia with ice-cold sterile RPMI medium, and cultured in RPMI 1640 supplemented with 40 ng/ml recombinant mouse M-CSF, 10% FCS, 1% penicillin/streptavidin and glutamine. Fresh M-CSF was added on day 3 and medium was refreshed on day 5. On day 7 cells were seeded and stimulated with 20 ng/ml ultrapure LPS (*Escherichia coli* 0111:B4 strain, InvivoGen) or 20 ng/ml ultrapure LPS (*E. coli* 0111:B4 strain, Invivogen) for 3 h followed by 5 mM ATP (Sigma-Aldrich) for 20 min for NLRP3 activation.

Cytokine detection. Cytokine concentrations in culture medium were determined by magnetic bead-based multiplex assay using Luminex technology (Bio-Rad), IL-1β ELISA (Affymetrix eBioscience), IL-18 ELISA (Biotechne - R & D Syst. Eur.), according to the manufacturers' instructions.

Immunoprecipitation studies. BMDMs were stimulated with human Flag–TNF (1 μg/ml) (VIB Protein Service Facility) as indicated. Cells were lysed in NP40 buffer (150 mM NaCl, 1% NP40, 10% glycerol and 10 mM Tris–HCl pH 8) and FLAG pulldown was performed using M2 beads (Sigma). The TNF-R1

signaling complex was eluted from beads using 3×FLAG peptide (Sigma) as described in the manufacturer's instructions. For USP2 and PPase treatment, the beads were incubated with 24 μg ml−1 USP2 (Enzo Life Sciences) and 8 U μl−1 λPPase (NEB) for 30 min at 37 °C before FLAG peptide elution.

Cell death assay. For cell death analysis in MEFs, cells were seeded the day before at 1×10^4 per well in triplicates in a 96-well plate. The next day, cells were stimulated with the indicated concentration of mTNF in the presence of 2.5 μM SytoxGreen (Invitrogen). SytoxGreen intensity was measured at intervals of one hour using a Fluostar Omega fluorescence plate reader, with an excitation filter of 485 nm and an emission filter of 520 nm, gains set at 1, 100, 20 flashes per well and orbital averaging with a diameter of 3 mm. For pyroptosis assay in BMDMs, cells were seeded the day before at 2.5×10^4 per well in triplicates in a 96-well plate. The next day, cells were stimulated with the indicated concentration of LPS and ATP in the presence of 0.25 μM SytoxGreen (Molecular probes). SytoxGreen intensity was measured at intervals of 5 min, for a total of 1 h, using a Incucyte device (EssenbioScience). Percentage of cell death was calculated as (induced fluorescence − background fluorescence)/(maximum fluorescence − background fluorescence) × 100. The maximal fluorescence is obtained by full permeabilization of the cells by using Triton X-100 at a final concentration of 0.1 %. All cell death data are presented as mean ± SEM of n (indicated in the figure) independent experiments, unless stated otherwise.

Immunoblot analysis. Cells and tissue extracts were prepared in E1A lysis buffer (250 mM NaCl, 50 mM Tris pH 7.4, 0.1% NP-40) containing a complete protease inhibitor cocktail (1:25) (Roche) and centrifuged for 10 min at 14,000 rpm in a microcentrifuge at 4°C or were directly lysed in 2× Laemlli buffer. For cleaved Caspase 1 immunoblotting, cell lysates and culture supernatants were incubated with cell lysis buffer (20 mM Tris HCl pH 7.4, 200 mM NaCl, 1% NP-40) and denatured in Laemmli buffer. Supernatants were separated by SDS-polyacrylamide gel electrophoresis (PAGE), transferred to nitrocellulose and immunodetected with anti-IκBα (Santa Cruz Biotechnology, Inc., sc-371), anti-phospho-IκBα (Cell Signaling, CST9246), anti-A20 (Santa Cruz Biotechnology, Inc., sc-166692), anti-p38 (Cell Signaling, CST9212), anti-phospho-p38 (Cell Signaling, CST9215), anti-Caspase3 (Cell Signaling, CST9662), anti-SAPK/JNK (Cell Signaling, CST9252), anti-phospho-SAPK/JNK (Cell Signaling, CST4668), anti-caspase-1 (Adipogen, AG-20B-0042), anti-β-tubulin (Sigma-Aldrich, T4026) and anti-β-actin (Santa Cruz Biotechnology, Inc., sc-47778) antibodies.

In vivo TNF toxicity. Mice were injected i.p. with a sublethal dose of mouse TNF (5 μg mouse TNF/20 g mouse). *E. coli*-expressed recombinant mTNF was produced and purified to homogeneity in our

laboratory, and endotoxin levels did not exceed 1 ng/mg protein. Body temperature and survival were monitored every hour. In a separate experiment, mice were euthanized after 2 h (A20^{ZnF7}) or 5 h (*Tnfaip3*$^{ZnF4ZnF7/ZnF4ZnF7}$*Vil1*-Cre) for histological analysis.

Induction of DSS-induced colitis and clinical score. Acute colitis was induced by addition of 1.5 % dextran sodium sulphate (DSS, 36–50 kDa; MP Biomedicals) to the drinking water for 5 days. Body weight, stool consistency and fecal blood were determined daily. Fecal blood was determined using Hemoccult SENSA (Beckman Coulter) analysis. The baseline clinical score was determined on day 0. In brief, no weight loss was scored as 0, weight loss of 1–5 % from baseline as 1, 5–10 % as 2, 10–20 % as 3, and >20 % as 4. For bleeding, a score of 0 was assigned for no blood, 2 for positive hemoccult, and 4 for gross bleeding. For stool consistency, a score of 0 was assigned for well-formed pellets, pasty and semi-formed stools were scored as 2, and liquid stools as 4. The average of these 3 scores was used as total clinical score, ranging from 0 (healthy) to 4 (maximal colitis).

FITC–dextran intestinal permeability assay. Intestinal permeability was assessed by oral gavage of FITC–dextran (MW: 3000-5000, Sigma). Mice were administered 12 mg of FITC-dextran per 20 g body weight in sterile PBS by oral gavage. After 4 h, blood was collected from the facial vein, and FITC–dextran concentrations were measured in 50 µl of serum by fluorometry (485 nm). Mice were anesthetized during blood collection. Serial dilutions of FITC–dextran in PBS were used each time to generate a standard curve and serum from PBS-gavaged mice was used as blanks.

Clinical scoring for arthritis development. The severity of arthritis was assessed using a visual scoring system. Mice were scored every two weeks for development of peripheral arthritis. A score ranging from 0 to 3 was assigned to each paw, with 0 being normal, 0.5 being swelling of one or more toes, 1 being mild swelling of the wrist and/or ankle or carpus and/or tarsus, 2 being moderate swelling of the wrist and/or ankle or carpus and/or tarsus or mild swelling of both, and 3 being severe swelling of the entire paw.

Quantitative real-time PCR. Total RNA was isolated using TRIzol reagent (Invitrogen) and Aurum Total RNA Isolation Mini Kit (Biorad), according to manufacturer's instructions. Synthesis of cDNA was performed using iScript cDNA synthesis kit (BioRad) according to the manufacturer's instructions. cDNA was amplified on quantitative PCR in a total volume of 5 µl with SensiFAST SYBR® No-ROX Kit (Bioline) and specific primers on a LightCycler 480 (Roche). The reactions were performed in triplicates. The following mouse-specific primers were used: *Rpl13a* forward, 5'-CCTGCTGCTCTCAAGGTT-3'; *Rpl13a* reverse, 5'-TGGTTGTCACTGCCTGGTACTT-3'; *Rpl13a* forward, 5'-AGTGTTGGATACAGGCCAGAC-3'; *Rpl13a* reverse, 5'-CGTGATTCAAATCCCTGAAGT-3'; *Tnf* forward, 5'-

ACCCTGGTATGAGCCCATATAC-3'; *Tnf* reverse, 5'-ACACCCATTCCCTTCACAGAG-3'*; Il1b* forward, 5'-CACCTCACAAGCAGAGCACAAG-3'; *Il1b* reverse, 5'-GCATTAGAAACAGTCCAGCCCATAC-3'; *Il6* forward, 5'-GAGGATACCACTCCCAACAGACC-3'; *Il6* reverse, 5'-AAGTGCATCATCGTTGTTCATACA-3'; *Il18* forward, 5'-CAGGCCTGACATCTTCTGCAA-3'; *Il18* reverse, 5'-TCTGACATGGCAGCCATTGT-3'.

Flow cytometry. Spleens were isolated and processed to a single-cell suspension. 5×10^6 splenocytes were stained with a combination of the following fluorochrome- or biotin-labeled monoclonal antibodies: CD3 (Thermo Fisher Scientific, 145-2c11 or 17A2), CD4 (BD Biosciences, GK1.5), CD8 (Thermo Fisher Scientific, 53-6.7), CD11b (BD Biosciences, M1/70), CD11c (Thermo Fisher Scientific, N418), CD16/32 (Bioceros, 2.4G2), CD19 (Thermo Fisher Scientific, 1D3), CD62L (BD Biosciences, MEL-14), CD64 (BioLegend, X54-5/7.1), F4/80 (BioLegend, BM8), Ly6C (Thermo Fisher Scientific, HK1.4), Ly6G (BD Biosciences, 1A8), NK1.1 (BD Biosciences, PK136), SiglecF (BD Biosciences, E50-2440), and TNF (BD Biosciences, MP6-XT22). Intracellular staining for TNF was performed with the Foxp3 kit (eBioscience, 00-5523-00). Cell viability was measured using an eFluor 506 (eBioscience, 65-0866-18) or eFluor780 (eBioscience, 65-0865-14) fixable viability dye. Absolute cell counts were determined by use of 123 count ebeads (eBioscience, 01-1234-42). Samples were measured on a FACS Fortessa 5 laser or BD FACSymphony (BD Biosciences) and data were analyzed using FlowJo.

Ex vivo cytokine production. To assess intracellular TNF production, 5×10^6 splenocytes were cultured in DMEM (Gibco) supplemented with 10% FCS (Bodinco) in the presence of monensin (420701, BioLegend) and brefeldinA (420601, Biolegend) and incubated 3.5 h at 37°C.

Statistics. Results are expressed as the mean ± SEM or mean ± SD, as indicated in figure legend. Statistical significance between experimental groups was assessed using a nonparametric Mann–Whitney U-statistical test. Statistical significance between multiple groups was assessed using either one- or two-way ANOVA with Tukey correction for multiple comparison. Comparison of 2 or more groups over time was analysed as longitudinal data (repeated measurements over time) using the residual maximum likelihood (REML) as implemented in Genstat v19[30]. Briefly, a linear mixed model (random terms underlined) of the form response = μ + genotype + time + genotype.time + subject.time was fitted to the longitudinal data. The term subject.time represents the residual error term with dependent errors because the repeated measurements are taken repeatedly from the same subjects, causing correlations among observations. Times of measurement were set as equally spaced, and the best correlation model was selected based on the Aikake Information Coefficient (AIC). Significance of genotype effects over time (i.e. genotype.time) and changes in differences between genotype effects over time were assessed by an approximate F-test, of which the

denominator degrees of freedom were calculated using algebraic derivatives as implemented in Genstat v19[30].

Data availability statement. All data supporting the findings of this study are available from the corresponding author on reasonable request.

Methods-only references

26 Clausen, B. E., Burkhardt, C., Reith, W., Renkawitz, R. & Forster, I. Conditional gene targeting in macrophages and granulocytes using LysMcre mice. *Transgenic Res* **8**, 265-277 (1999).

27 Madison, B. B. *et al.* Cis elements of the villin gene control expression in restricted domains of the vertical (crypt) and horizontal (duodenum, cecum) axes of the intestine. *J Biol Chem* **277**, 33275-33283, doi:10.1074/jbc.M204935200 (2002).

28 Adachi, O. *et al.* Targeted disruption of the MyD88 gene results in loss of IL-1- and IL-18-mediated function. *Immunity* **9**, 143-150 (1998).

29 Armaka, M., Ospelt, C., Pasparakis, M. & Kollias, G. The p55TNFR-IKK2-Ripk3 axis orchestrates arthritis by regulating death and inflammatory pathways in synovial fibroblasts. *Nat Commun* **9**, 618, doi:10.1038/s41467-018-02935-4 (2018).

30 Baird, D., Murray, D., Payne, R. & Soutar, D. An Introduction to GenStat for Windows (19th Edition). *Genstat* **Vol. 19** (2017).

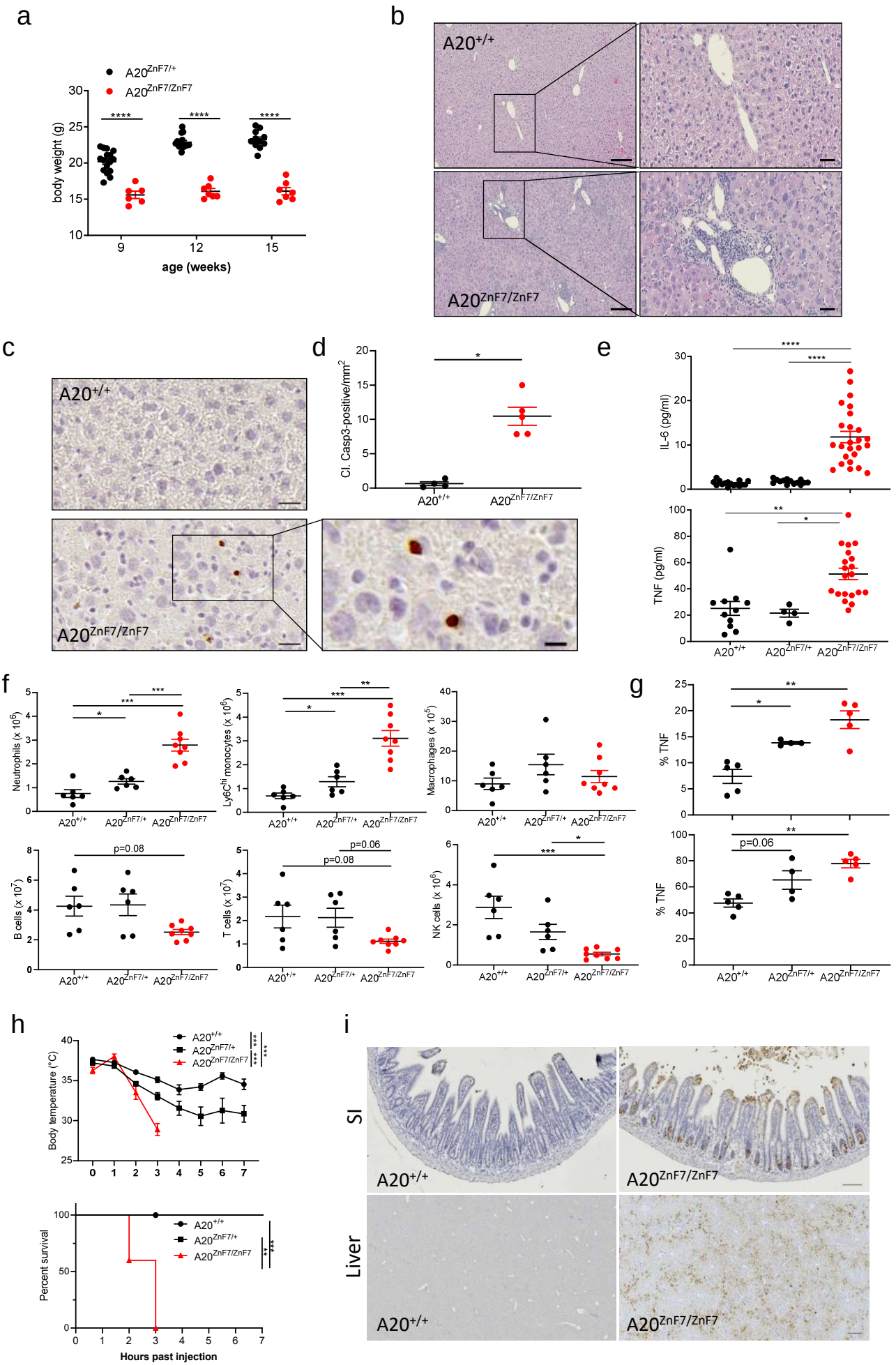
a
A20ZnF7/+
A20ZnF7/ZnF7
body weight (g)
age (weeks)
b
A20+/+
A20ZnF7/ZnF7
c
A20+/+
A20ZnF7/ZnF7
d
Cl. Casp3-positive/mm2
e
IL-6 (pg/ml)
TNF (pg/ml)
f
Neutrophils (x 10^6)
Ly6Chi monocytes (x 10^6)
Macrophages (x 10^5)
B cells (x 10^7)
T cells (x 10^7)
NK cells (x 10^6)
p=0.08
p=0.06
g
% TNF
h
Body temperature (°C)
Percent survival
Hours past injection
i
SI
Liver

Figure 1

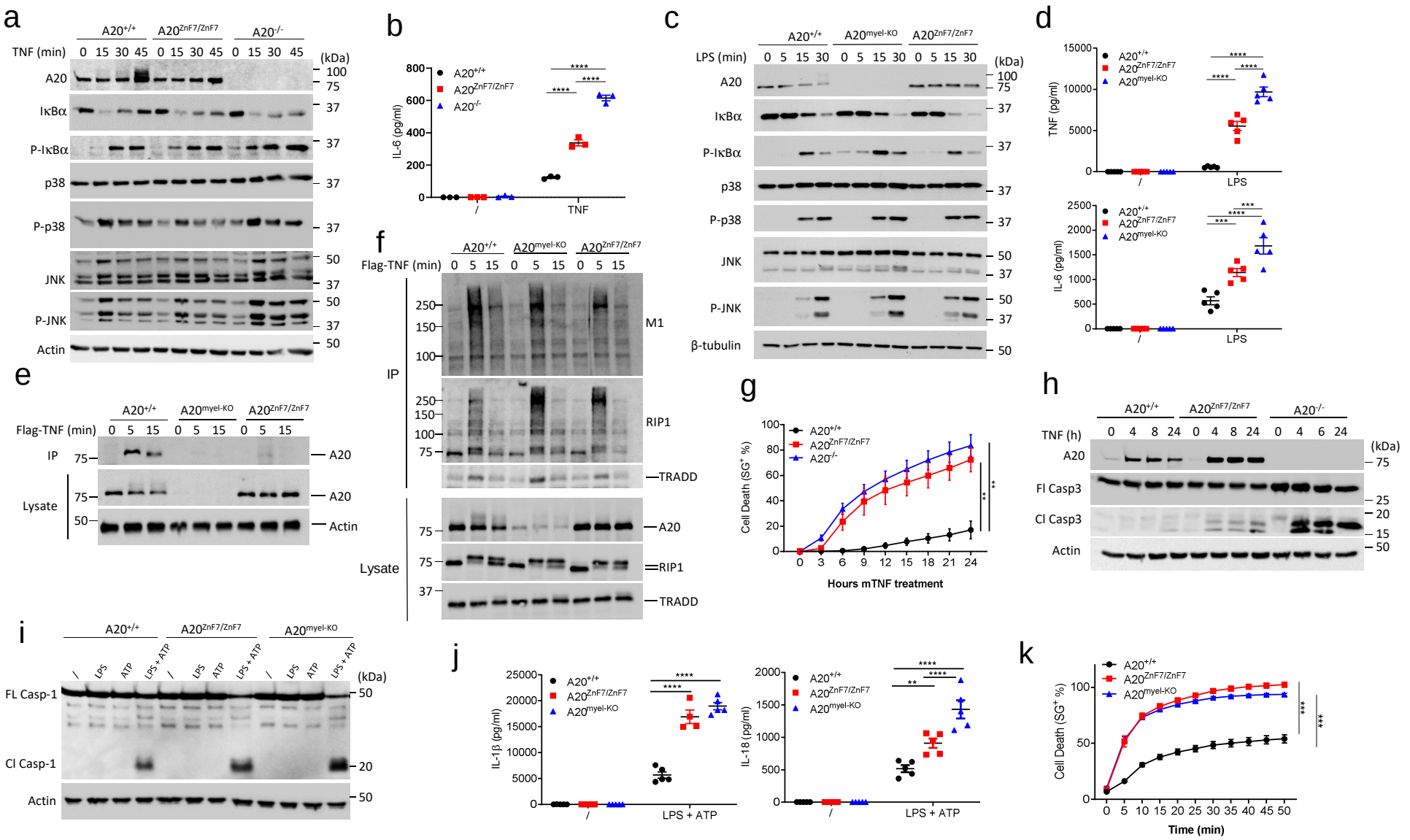
a
A20+/+
A20ZnF7/ZnF7
A20-/-
TNF (min)
0 15 30 45 0 15 30 45 0 15 30 45
(kDa)
A20
IκBα
P-IκBα
p38
P-p38
JNK
P-JNK
Actin
100
75
37
37
37
50
37
50
37
50
b
IL-6 (pg/ml)
800
600
400
200
0
A20+/+
A20ZnF7/ZnF7
A20-/-
****
****
****
/
TNF
c
A20+/+
A20myel-KO
A20ZnF7/ZnF7
LPS (min)
0 5 15 30 0 5 15 30 0 5 15 30
(kDa)
A20
IκBα
P-IκBα
p38
P-p38
JNK
P-JNK
β-tubulin
100
75
37
37
37
50
37
50
37
50
d
TNF (pg/ml)
15000
10000
5000
0
A20+/+
A20ZnF7/ZnF7
A20myel-KO
****
****
****
/
LPS
IL-6 (pg/ml)
2500
2000
1500
1000
500
0
A20+/+
A20ZnF7/ZnF7
A20myel-KO
***
****
***
/
LPS
e
A20+/+
A20myel-KO
A20ZnF7/ZnF7
Flag-TNF (min)
0 5 15 0 5 15 0 5 15
IP
75
A20
Lysate
75
A20
50
Actin
f
A20+/+
A20myel-KO
A20ZnF7/ZnF7
Flag-TNF (min)
0 5 15 0 5 15 0 5 15
IP
250
150
100
M1
250
150
100
75
RIP1
TRADD
Lysate
75
A20
75
RIP1
37
TRADD
g
Cell Death (SG+ %)
100
80
60
40
20
0
A20+/+
A20ZnF7/ZnF7
A20-/-
**
**
0 3 6 9 12 15 18 21 24
Hours mTNF treatment
h
A20+/+
A20ZnF7/ZnF7
A20-/-
TNF (h)
0 4 8 24 0 4 8 24 0 4 6 24
(kDa)
A20
Fl Casp3
Cl Casp3
Actin
75
25
20
15
50
i
A20+/+
A20ZnF7/ZnF7
A20myel-KO
/ LPS ATP LPS + ATP / LPS ATP LPS + ATP / LPS ATP LPS + ATP
(kDa)
FL Casp-1
Cl Casp-1
Actin
50
20
50
j
IL-1β (pg/ml)
25000
20000
15000
10000
5000
0
A20+/+
A20ZnF7/ZnF7
A20myel-KO
****
****
/
LPS + ATP
IL-18 (pg/ml)
2000
1500
1000
500
0
A20+/+
A20ZnF7/ZnF7
A20myel-KO
****
****
**
/
LPS + ATP
k
Cell Death (SG+ %)
100
50
0
A20+/+
A20ZnF7/ZnF7
A20myel-KO
***
***
0 5 10 15 20 25 30 35 40 45 50
Time (min)

Figure 2

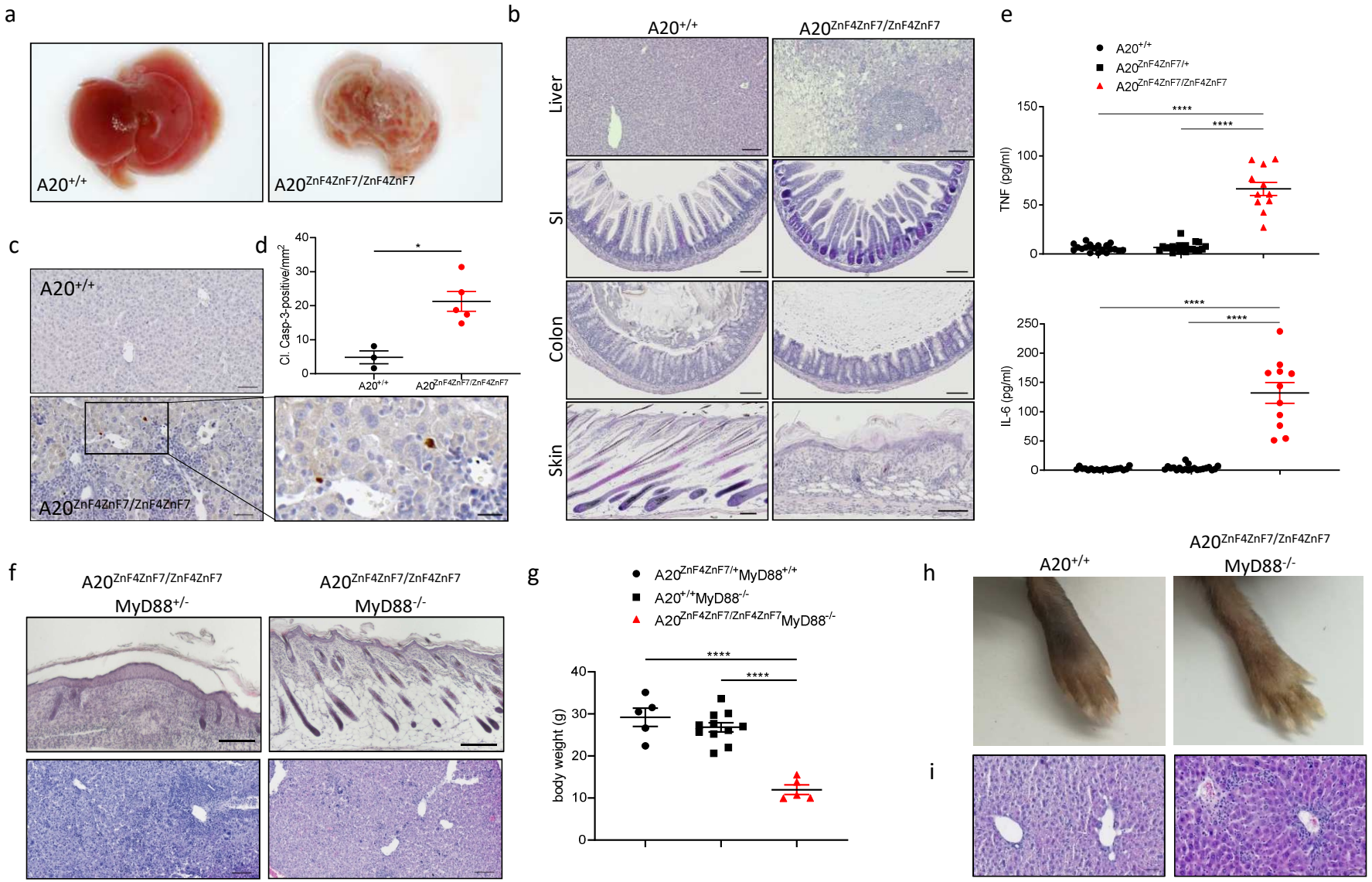
a
A20+/+
A20ZnF4ZnF7/ZnF4ZnF7
b
A20+/+
A20ZnF4ZnF7/ZnF4ZnF7
Liver
SI
Colon
Skin
c
A20+/+
A20ZnF4ZnF7/ZnF4ZnF7
d
Cl. Casp-3-positive/mm2
A20+/+
A20ZnF4ZnF7/ZnF4ZnF7
e
A20+/+
A20ZnF4ZnF7/+
A20ZnF4ZnF7/ZnF4ZnF7
TNF (pg/ml)
IL-6 (pg/ml)
f
A20ZnF4ZnF7/ZnF4ZnF7
MyD88+/-
A20ZnF4ZnF7/ZnF4ZnF7
MyD88-/-
g
A20ZnF4ZnF7/+MyD88+/+
A20+/+MyD88-/-
A20ZnF4ZnF7/ZnF4ZnF7MyD88-/-
body weight (g)
h
A20+/+
A20ZnF4ZnF7/ZnF4ZnF7
MyD88-/-
i

Figure 3

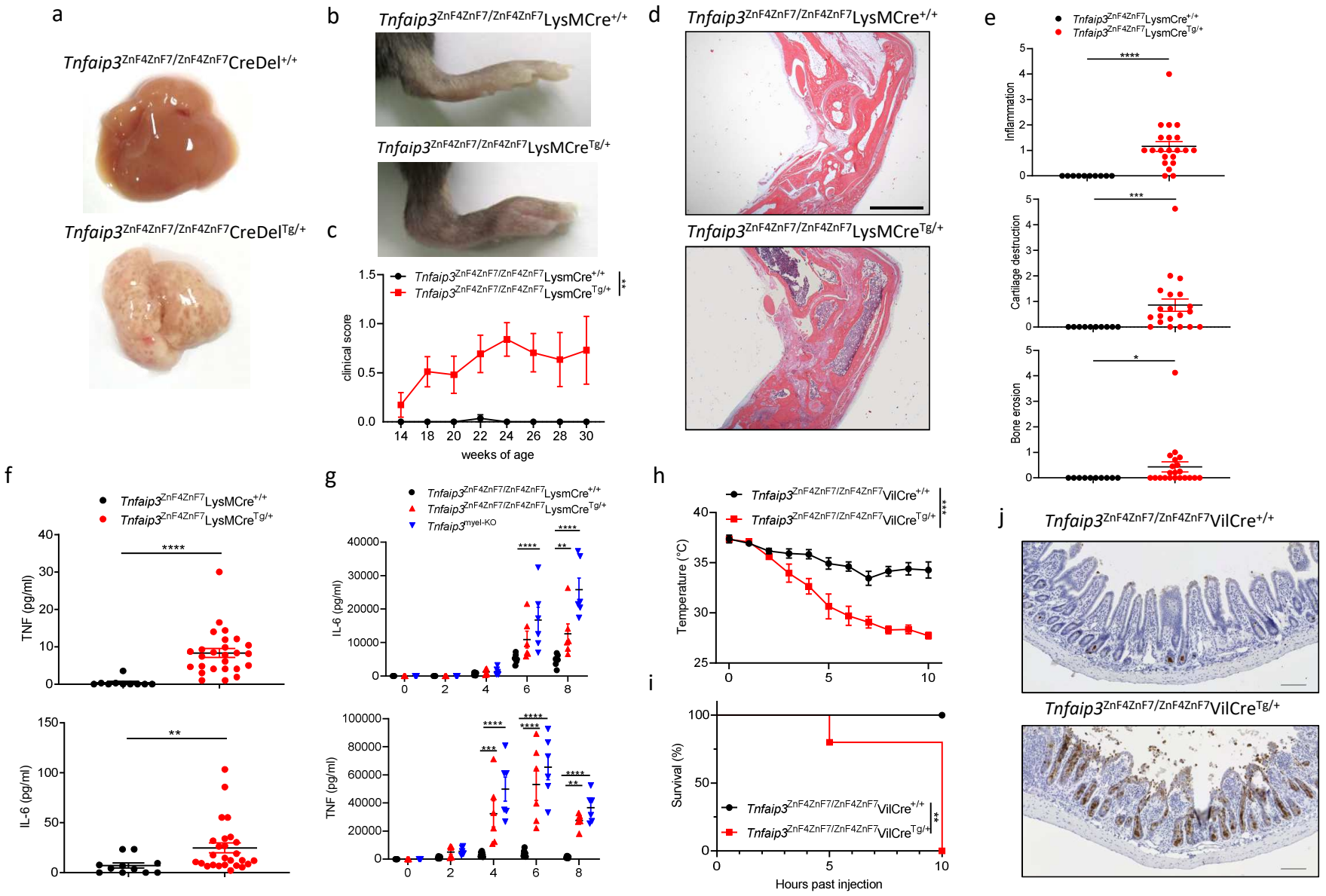
a
Tnfaip3ZnF4ZnF7/ZnF4ZnF7CreDel+/+
Tnfaip3ZnF4ZnF7/ZnF4ZnF7CreDelTg/+
b
Tnfaip3ZnF4ZnF7/ZnF4ZnF7LysMCre+/+
Tnfaip3ZnF4ZnF7/ZnF4ZnF7LysMCreTg/+
c
Tnfaip3ZnF4ZnF7/ZnF4ZnF7LysmCre+/+
Tnfaip3ZnF4ZnF7/ZnF4ZnF7LysmCreTg/+
clinical score
weeks of age
d
Tnfaip3ZnF4ZnF7/ZnF4ZnF7LysMCre+/+
Tnfaip3ZnF4ZnF7/ZnF4ZnF7LysMCreTg/+
e
Tnfaip3ZnF4ZnF7LysmCre+/+
Tnfaip3ZnF4ZnF7LysmCreTg/+
Inflammation
Cartilage destruction
Bone erosion
f
Tnfaip3ZnF4ZnF7LysMCre+/+
Tnfaip3ZnF4ZnF7LysMCreTg/+
TNF (pg/ml)
IL-6 (pg/ml)
g
Tnfaip3ZnF4ZnF7/ZnF4ZnF7LysmCre+/+
Tnfaip3ZnF4ZnF7/ZnF4ZnF7LysmCreTg/+
Tnfaip3myel-KO
IL-6 (pg/ml)
TNF (pg/ml)
h
Tnfaip3ZnF4ZnF7/ZnF4ZnF7VilCre+/+
Tnfaip3ZnF4ZnF7/ZnF4ZnF7VilCreTg/+
Temperature (°C)
i
Survival (%)
Tnfaip3ZnF4ZnF7/ZnF4ZnF7VilCre+/+
Tnfaip3ZnF4ZnF7/ZnF4ZnF7VilCreTg/+
Hours past injection
j
Tnfaip3ZnF4ZnF7/ZnF4ZnF7VilCre+/+
Tnfaip3ZnF4ZnF7/ZnF4ZnF7VilCreTg/+

Figure 4

Extended Data Figure legends

Extended Data Figure 1. A20^{ZnF7} knock-in mice. (a) Schematic depiction of the *A20/Tnfaip3* locus indicating the sequence of the single stranded oligonucleotide used for mutating the ZnF7 domain that was introduced by pronuclear injection into mouse zygotes, and sequencing result of the wild-type (WT) and of the targeted ZnF7 knock-in allele. Boxes indicate exons 3 to 9 (E3–E9). **(b)** Birth and survival rates of control (A20$^{+/+}$), A20$^{ZnF7/+}$ and A20$^{ZnF7/ZnF7}$ offspring from A20$^{ZnF7/+}$ x A20$^{ZnF7/+}$ breeding couples. **(c)** Gross appearance of A20$^{ZnF7/+}$ and A20$^{ZnF7/ZnF7}$ mice. **(d)** Representative pictures of spleen and inguinal lymph nodes from 28-week-old control (A20$^{+/+}$) and A20$^{ZnF7/ZnF7}$ littermate mice. **(e)** Representative pictures of hindpaws of 15-week-old control (A20$^{+/+}$) and A20$^{ZnF7/ZnF7}$ littermates, showing extensive swelling of the toes of the A20$^{ZnF7/ZnF7}$ mice. **(f)** Representative micro-CT pictures of hindpaws (left) and knees (right) of 28-week-old control (A20$^{+/+}$) and A20$^{ZnF7/ZnF7}$ littermates. **(g)** Representative hematoxylin-eosin-stained histological images of ankle joints (left) and toes (right) from 28-week-old control (A20$^{+/+}$) and A20$^{ZnF7/ZnF7}$ littermates. Scale bar, 500 µm.

Extended Data Figure 2. FACS immunophenotyping of spleen of control and A20^{ZnF7} mice. (a-c) General gating strategy as applied for immune cell populations described in Figure 1g. (a) Lymphocytes, singlets, live, CD3$^-$CD19$^+$ (B cells), CD3$^+$CD19$^-$ (T cells) and CD3$^-$CD19$^-$ NK1.1$^+$ (NK cells); (b) non-debris, singlets, live, lineage$^-$ (CD3$^-$CD19$^-$NK1.1$^-$), F4/80$^+$, CD64$^+$ and autofluorescent; (c) non-debris, singlets, live, lineage$^-$, Ly6G$^+$CD11b$^+$ (neutrophils) and Ly6G$^-$SiglecF$^-$Ly6C^{hi}CD11b+ (monocytes). FSC: forward scatter, SSC: side scatter, A: Area, H: height, W: width, L/D: live/dead. **(d-f)** Bar graphs representing absolute numbers of total (left) and naive (right) CD4 T cells (d), total (left) and naive (right) CD8 T cells (e) and yd T cells (f) as measured by flow cytometry in the spleens of A20$^{+/+}$, A20$^{ZnF/+}$ and A20$^{ZnF7/ZnF7}$ animals. Data are expressed as mean ± SEM. *, ** represent $p < 0.05$ and $p < 0.01$ (Two-sided non-parametric Mann-Whitney test between indicated genotypes).

Extended Data Figure 3. MyD88-dependent mechanisms contribute to the local inflammatory pathology in A20^{ZnF7} mice (a-b) Gross appearance (a) and bodyweight (b) of of 10 week-old A20$^{ZnF7/+}$MyD88$^{+/-}$, A20$^{ZnF7/ZnF7}$MyD88$^{+/-}$ and A20$^{ZnF7/ZnF7}$ MyD88$^{-/-}$ mice. Each dot represents a biologically independent mouse (A20$^{ZnF7/+}$MyD88$^{+/-}$, n=9; A20$^{ZnF7/ZnF7}$MyD88$^{+/+}$, n=13 and A20$^{ZnF7/ZnF7}$ MyD88$^{-/-}$, n=6). Data are expressed as mean ± SEM. * and **** represent $p<0.05$ and $p<0.0001$,

respectively (parametric two-way ANOVA between indicated genotypes). **(c)** Representative hematoxylin-eosin-stained sections of liver from 18-week-old $A20^{ZnF7/ZnF7}MyD88^{+/+}$ and $A20^{ZnF7/ZnF7}MyD88^{-/-}$ littermates. Scale bar, 50 μm. Picture representative for 3 biologically independent mice. **(d)** Representative pictures of hindpaws of 10-week-old $A20^{ZnF7/ZnF7}MyD88^{+/+}$ and $A20^{ZnF7/ZnF7}MyD88^{-/-}$ littermates. Pictures representative for 3 biologically independent mice **(e)** Levels of IL-6 and TNF in serum of $A20^{+/+}MyD88^{+/+}$, $A20^{+/+}MyD88^{-/-}$, $A20^{ZnF7/ZnF7}MyD88^{+/+}$ and $A20^{ZnF7/ZnF7}MyD88^{-/-}$ mice. Each dot represents a biologically independent mouse ($A20^{+/+}MyD88^{+/+}$, n=9; $A20^{+/+}MyD88^{-/-}$, n=3; $A20^{ZnF7/ZnF7}MyD88^{+/+}$, n=13 and $A20^{ZnF7/ZnF7}MyD88^{-/-}$, n=6). Data are expressed as mean ± SEM. *, ** represent $p<0.05$ and $p=0.0033$ respectively (parametric one-way ANOVA between indicated genotypes).

Extended Data Figure 4. ZnF7 is critical for A20-mediated suppression of inflammatory signaling. Western blot analysis of whole cell lysates from $A20^{+/+}$, $A20^{ZnF7/ZnF7}$ and $A20^{myel\text{-}KO}$ BMDMs stimulated with TNF as indicated**.** β-tubulin is shown as a loading control. Figure representative for 3 independent experiments.

Extended Data Figure 5. $A20^{ZnF4ZnF7}$ knock-in mice. (a) Schematic depiction of the *A20/Tnfaip3* locus indicating the position of ZnF4 and ZnF7 mutations. Boxes indicate exons 3 to 9 (E3–E9). Sequences of the donor vector, containing ~1kb 5' and 3' homologous arms around the Cys-to-Ala mutations used for mutating the ZnF4 and ZnF7 domains, that were introduced by pronuclear injection into mouse zygotes. Sequencing result of the wild-type (WT) allele and of the targeted ZnF4 and ZnF7 knock-in alleles. **(b)** Gross appearance of 2-week old control ($A20^{+/+}$), $A20^{ZnF4ZnF7/+}$ and $A20^{ZnF4ZnF7/ZnF4ZnF7}$ mice. **(c)** Gross appearance of 2-week old $A20^{ZnF4ZnF7/ZnF4ZnF7}MyD88^{-/-}$ mice compared to $A20^{ZnF4ZnF7/ZnF4ZnF7}MyD88^{+/-}$mice.

Extended Data Figure 6. Conditional 'floxed' $A20^{ZnF4/ZnF7}$ knock-in mice. (a) Targeting scheme showing the LoxP-flanked (Floxed) and knock-in A20 alleles. Boxes indicate exons 3 to 9 (E3-E9). LoxP sites are indicated by arrowheads. **(b)** Gross appearance of 2 week-old control (*Tnfaip3*$^{ZnF4ZnF7/ZnF4ZnF7}$CreDel$^{+/+}$) and *Tnfaip3*$^{ZnF4ZnF7/ZnF4ZnF7}$CreDel$^{Tg/+}$ littermate mice. **(c)** Representative histological images of ankle joints from 30-week-old littermate mice with the indicated genotypes. Bone erosion was detected by tartrate-resistant acid phosphatase (TRAP) staining of osteoclast

activity, and cartilage destruction was assessed by proteoglycan staining with toluidine blue. H/E, haematoxylin and eosin. Scale bar: 500 µm. Pictures representative for 5 biologically independent mice. **(d)** Clinical score, based on loss in body weight, stool consistency, and presence of fecal blood, of 30 week-old *Tnfaip3*$^{ZnF4ZnF7/ZnF4ZnF7}$vilCre$^{Tg/+}$ (n=4) and control (*Tnfaip3*$^{ZnF4ZnF7/ZnF4ZnF7}$vilCre$^{+/+}$**,** n=4) littermate mice treated with 1.5 % DSS. The experiment was stopped at day 5 since *Tnfaip3*$^{ZnF4ZnF7/ZnF4ZnF7}$vilCre$^{Tg/+}$ started dying. Data are expressed as mean ± SEM. * represents p=0.0204 (2-way ANOVA with Sidak's multiple comparison) **(e)** Intestinal permeability assay using FITC-labelled dextran in 30-week-old *Tnfaip3*$^{ZnF4ZnF7/ZnF4ZnF7}$vilCre$^{Tg/+}$ (n=4) and control (*Tnfaip3*$^{ZnF4ZnF7/ZnF4ZnF7}$vilCre$^{+/+}$**,** n=4) mice before and after 5 days of DSS treatment. Data are expressed as mean ± SEM. * represents p=0.0143 (2-way ANOVA with Sidak's multiple comparison)

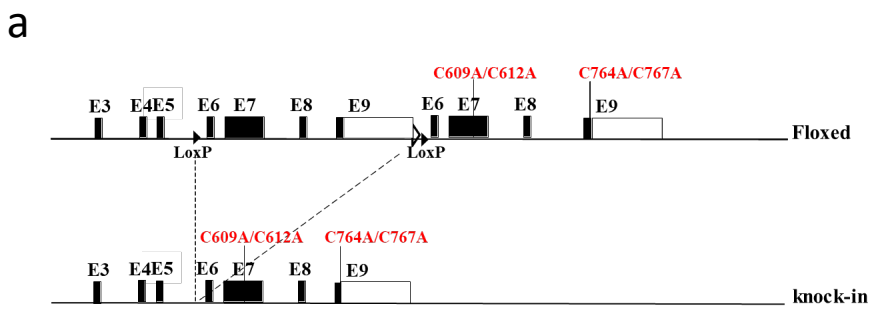

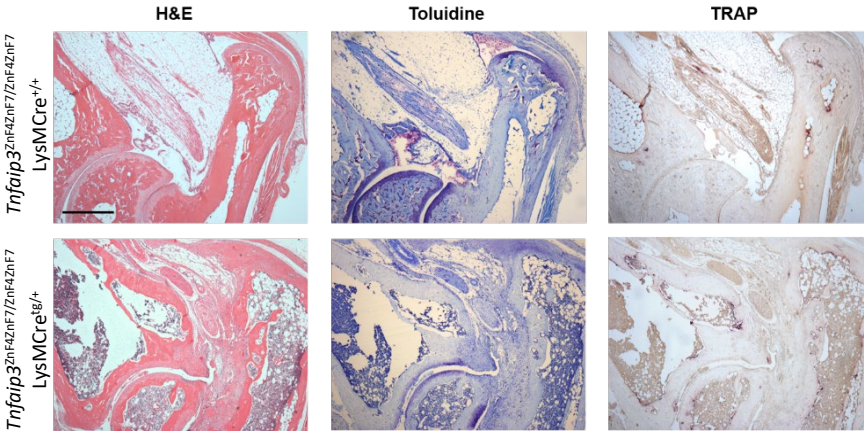

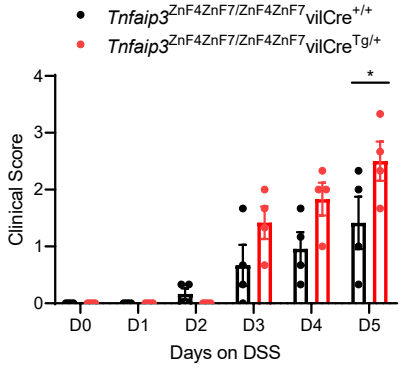

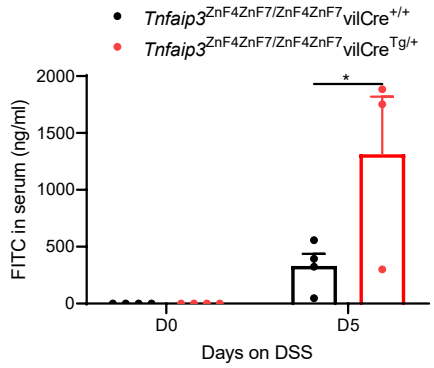

Extended Data Figure 6

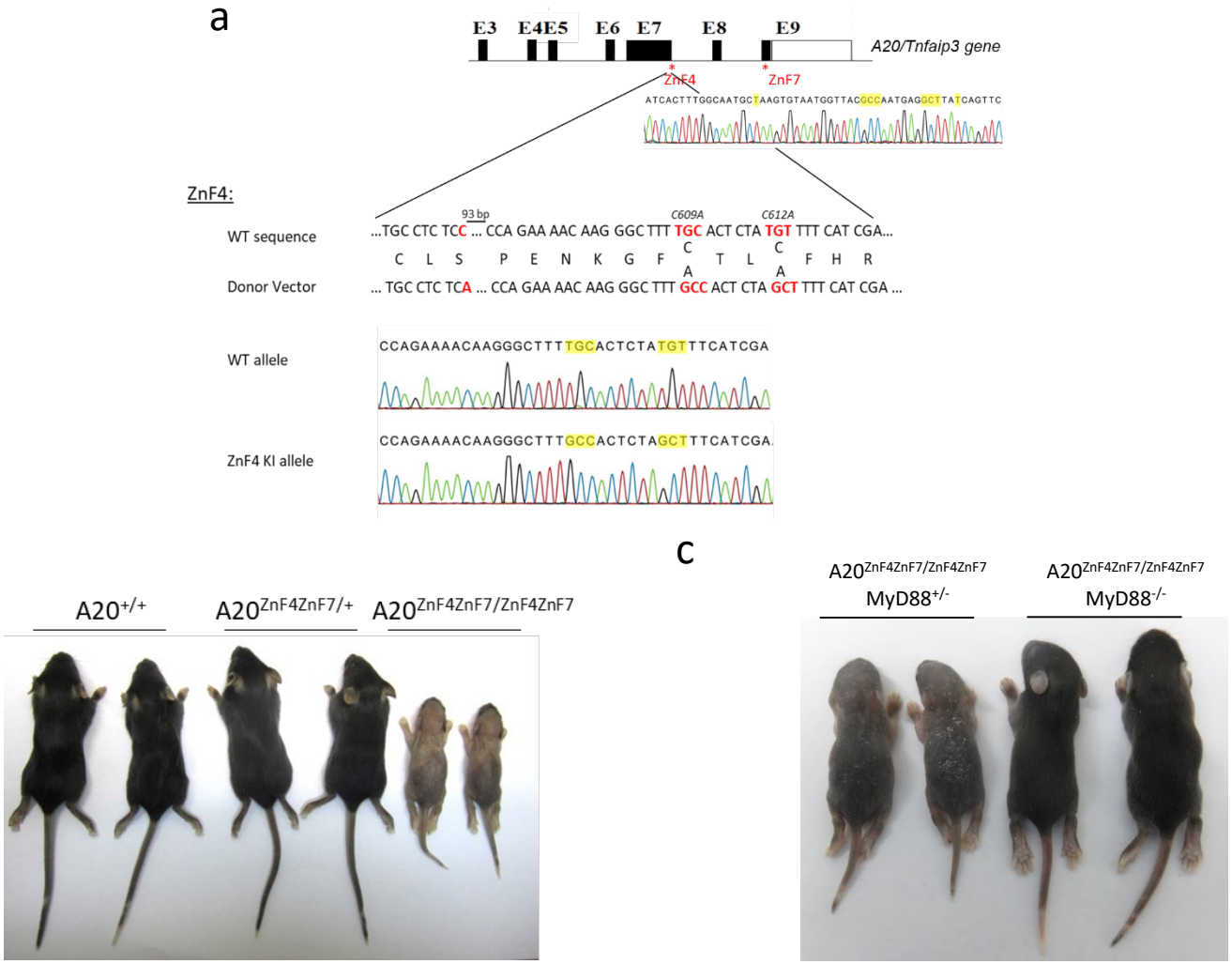

Extended Data Figure 5

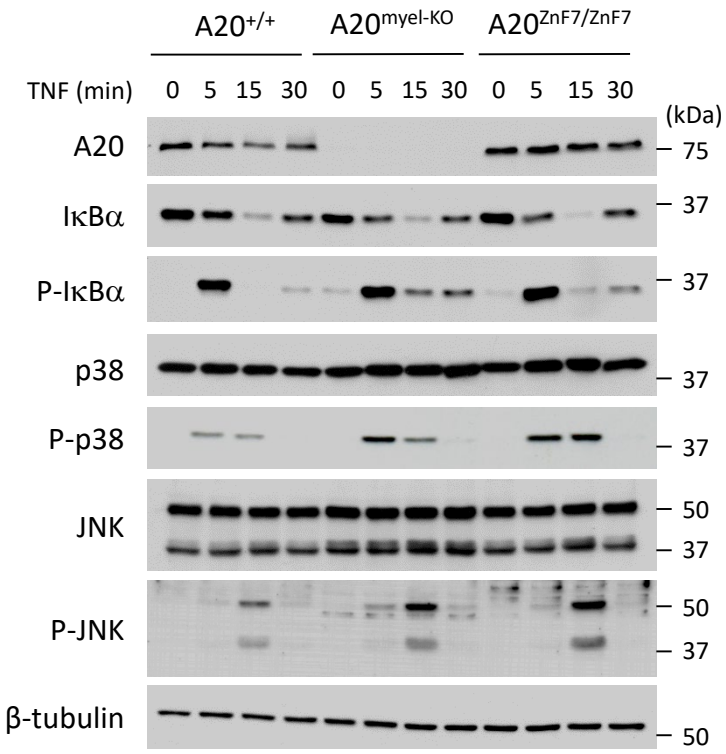

Extended Data Figure 4

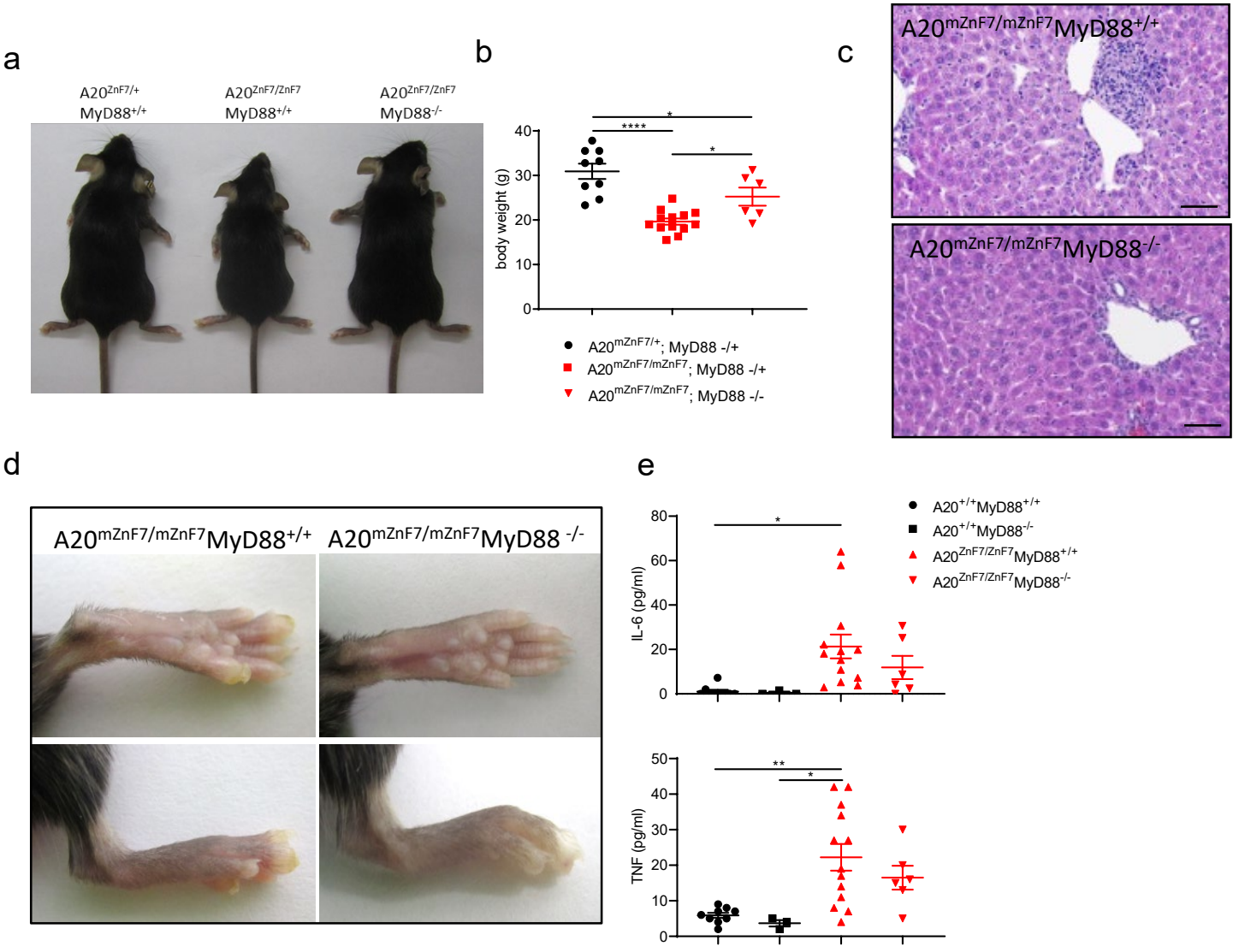

Extended Data Figure 3

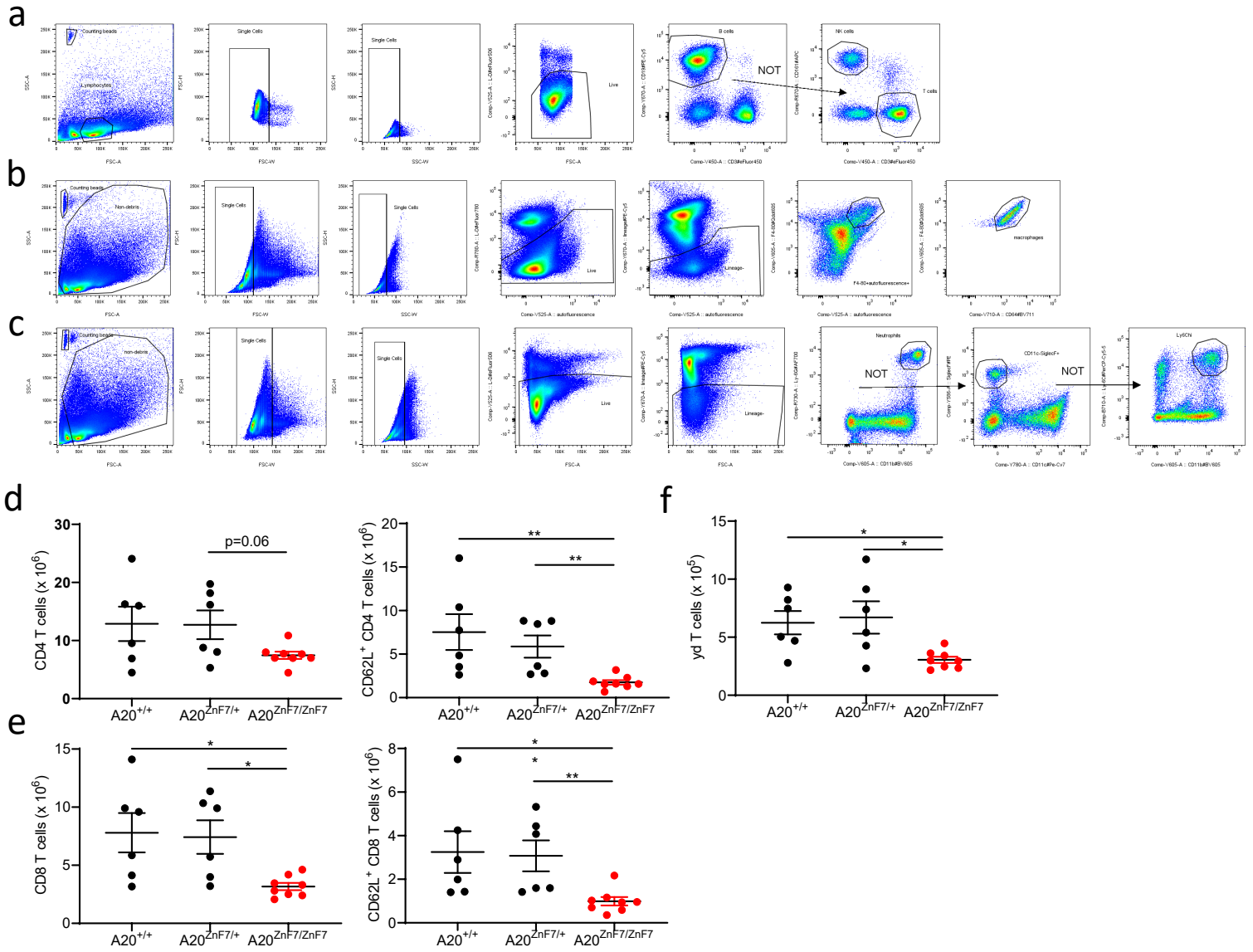

Extended Data Figure 2

a

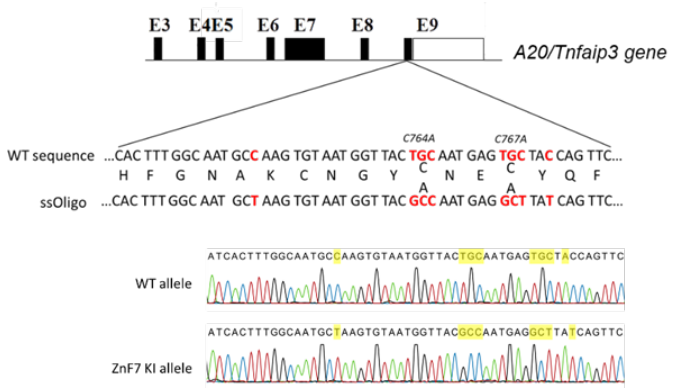

b

Genotype	Expected	Observed (at birth)	Observed (at weaning)
$A20^{+/+}$	25 % (41)	41	41
$A20^{ZnF7/+}$	50 % (83)	82	82
$A20^{ZnF7/ZnF7}$	25 % (41)	43	43
Total (observed)	100 % (166)	166	166

c

d

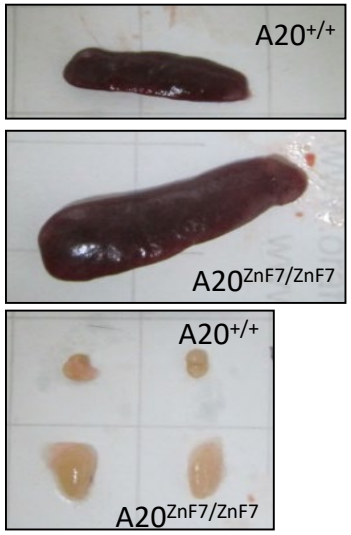

e

f

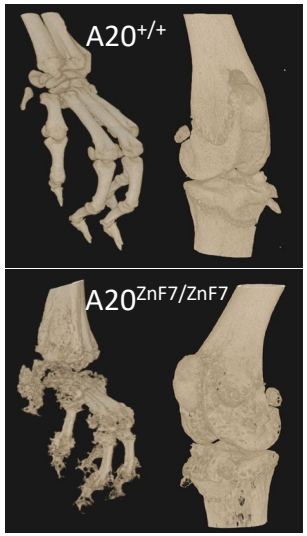

g

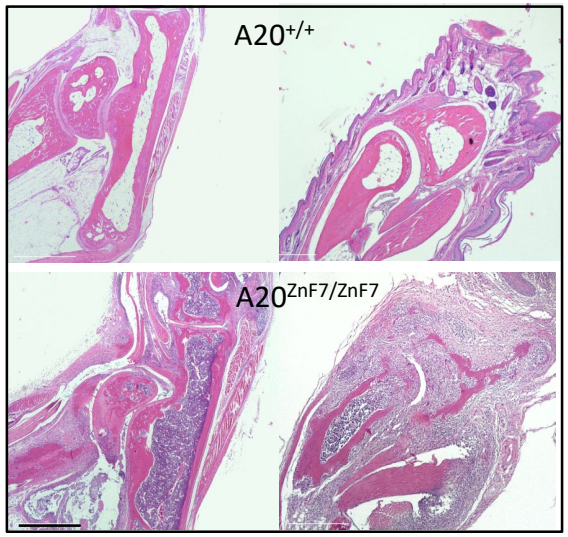

Extended Data Figure 1